eLife

Biochemistry and Chemical Biology
Structural Biology and Molecular Biophysics

Ligand Response of Guanidine-IV riboswitch at Single-molecule Level

Reviewed Preprint
v2 • June 3, 2024
Revised by authors

Reviewed Preprint
v1 • March 19, 2024

Lingzhi Gao, Dian Chen, Yu Liu

State Key Laboratory of Microbial Metabolism, School of Life Sciences and Biotechnology, Shanghai Jiao Tong University, Shanghai 200240, China • Shanghai Artificial Intelligence Laboratory, Shanghai 200232, China

Abstract

Riboswitches represent a class of non-coding RNA that possess the unique ability to specifically bind ligands and, in response, regulate gene expression. A recent report unveiled a type of riboswitch, known as the guanidine-IV riboswitch, which responds to guanidine levels to regulate downstream genetic transcription. However, the precise molecular mechanism through which the riboswitch senses its target ligand and undergoes conformational changes remain elusive. This gap in understanding has impeded the potential applications of this riboswitch. To bridge this knowledge gap, our study investigated the conformational dynamics of the guanidine-IV riboswitch RNA upon ligand binding. We employed single-molecule fluorescence resonance energy transfer (smFRET) to dissect the behaviors of the aptamer, terminator, and full-length riboswitch. Our findings indicated that the aptamer portion exhibited higher sensitivity to guanidine compared to the terminator and full-length constructs. Additionally, we utilized Position-specific Labelling of RNA (PLOR) combined with smFRET to observe, at the single-nucleotide and single-molecule level, the structural transitions experienced by the guanidine-IV riboswitch during transcription. Notably, we discovered that the influence of guanidine on the riboswitch RNA's conformations was significantly reduced after the transcription of 88 nucleotides. Furthermore, we proposed a folding model for the guanidine-IV riboswitch in the absence and presence of guanidine, thereby providing insights into its ligand-response mechanism.

Impact statement

The aptamer domain of the guanidine-IV riboswitch exhibits a greater sensitivity to guanidine, surpassing that observed in both the terminator and full-length riboswitch. A finely-tuned transcriptional window of the guanidine-IV riboswitch was detected to be responsive to ligand binding. Furthermore, a folding-function model for the guanidine-IV riboswitch under both guanidine-free and guanidine-present conditions offers valuable insights into its regulatory mechanism.

eLife assessment

This study presents **valuable** findings on the ligand- and ion-dependent structural dynamics of a transcriptional riboswitch. The single-molecule data presented are **solid** and prompts intriguing hypotheses and models, which will undoubtedly stimulate future structural analyses. These findings are of considerable interest to biochemists and biophysicists engaged in the study of RNA structure and riboswitch mechanisms.

https://doi.org/10.7554/eLife.94706.2.sa3

Introduction

Riboswitches, located at the 5'-untranslated region of mRNA, are capable of regulating gene expression through structural changes after binding to their specific ligands (Jones & Ferre-D'Amare, 2017; Mandal & Breaker, 2004; Serganov & Nudler, 2013; Sherlock & Breaker, 2020). A typical riboswitch consists of an aptamer domain and an expression platform. The aptamer domain binds to a specific ligand, leading to structural changes and regulation of gene expression (Garst et al., 2011; Kavita & Breaker, 2023; Winkler & Breaker, 2003). To date, more than 55 classes of riboswitches have been identified that can sense a diverse range of ligands, including small metabolites, anions, cations, amino acids, and nucleotides (Breaker, 2022; McCown et al., 2017). Furthermore, riboswitches responding to the same ligands have been found to exhibit distinct consequences and structures. For instance, there are four types of guanidine riboswitches, namely guanidine-I, guanidine-II, guanidine-III, and guanidine-IV riboswitch, which specifically bind to guanidine. Notably, the guanidine-IV riboswitch differs significantly from other guanidine riboswitches (Battaglia & Ke, 2018; L. Huang et al., 2017; Lin Huang et al., 2017; Lenkeit et al., 2020; Nelson et al., 2017; Salvail et al., 2020). Specifically, the guanidine-IV riboswitch is able to enhance the transcription of *mepA* by forming an anti-terminator structure upon guanidine binding. This structure plays a crucial role in exporting guanidine and reducing its toxicity in cells, making the guanidine-IV riboswitch a potential target for antibiotics (Kermani et al., 2018). Although the atomic-resolution structures of the guanidine-IV riboswitch have not been solved, it is proposed that a kissing loop (KL) forms in the riboswitch in the presence of guanidine. This KL facilitates the dissociation of the terminator and promotes transcriptional read-through (Lenkeit et al., 2020; Salvail et al., 2020). KL or pseudoknot formation upon ligand binding is a common occurrence in various riboswitches, including adenine, guanine, ZTP, pre-Q1, fluoride, and c-di-AMP riboswitches (Jones & Ferre-D'Amare, 2017; Lenkeit et al., 2020; Salvail et al., 2020). However, the mechanism by which KL affects gene expression in a transcriptional riboswitch, particularly during transcription, remains elusive.

The folding of RNA during transcription plays a critical role in its function, especially in riboswitches involved in gene regulation. Previous studies have investigated the co-transcriptional folding of various riboswitches using different techniques. For instance, Frieda *et al.* employed the optical-trapping assay to examine the co-transcriptional folding of an adenine riboswitch at the single-molecule resolution (Frieda & Block, 2012). Helmling *et al.* and Binas *et al.*, on the other hand, used NMR to map the transcriptional intermediates of the 2'-deoxyguanosine (2'-dG) and ZMP riboswitches at the single-nucleotide resolution (Binas et al., 2020; Helmling et al., 2017). Landgraf *et al.* utilized NMR and computational modeling to identify the ligand-sensing transcriptional window for the c-di-GMP and c-GAMP riboswitches (Landgraf et al., 2022). Hua *et al.* investigated the co-transcriptional folding of the twister ribozyme and the ZTP riboswitch by

mimicking the folding process using helicases to dissociate an RNA-DNA hybrid (Hua et al., 2020; Hua et al., 2018). Lou & Woodson, Uhm *et al*., Widom *et al*., and Yadav *et al*. employed the single-molecule fluorescence resonance energy transfer (smFRET) strategy to study the co-transcriptional folding of the *glmS* ribozyme, TPP, pre-Q1, and fluoride riboswitches by assembling transcriptional complexes (Lou & Woodson, 2024; Uhm et al., 2018; Widom et al., 2018; Yadav et al., 2022). Xue *et al*. monitored the folding of a growing SAM-VI riboswitch at the single-molecule resolution by FRET (Xue et al., 2023). Despite these previous investigations, there is lack of information regarding the conformational changes and ligand-sensing behavior of the guanidine-IV riboswitch during transcription. In this study, we used position-specific labeling of RNA (PLOR) to introduce a FRET pair, Cy3 and Cy5, at sites 78 and 35, respectively (Liu et al., 2018; Liu et al., 2015). Subsequently, we examined the ligand and Mg^{2+} responses of the aptamer domain, terminator/anti-terminator, and full-length guanidine-IV riboswitch using smFRET. Our findings revealed that both guanidine and Mg^{2+} facilitated the formation of a KL in the aptamer domain and significantly increased the KL-formed conformation in that domain. Interestingly, unlike the aptamer domain, the addition of guanidine and Mg^{2+} only had a minimal effect on the formation of the KL-formed anti-terminator structure in the terminator/anti-terminator or full-length RNA. Additionally, we mimicked the conformational changes and ligand-sensing behavior from the aptamer domain to the terminator sequence of the guanidine-IV riboswitch during transcription using smFRET and PLOR. The formation of the KL increased as the riboswitch was transcribed up to 88 nucleotides (corresponding to the aptamer), but decreased as the riboswitch was transcribed from 88 to 105 nucleotides (corresponding to the terminator). Based on our data, it became evident that the transcriptional fate did not determined by the terminator sequence, but rather by the aptamer region, which exhibited distinct ligand-sensing abilities.

Results

The construction and characteristics of the guanidine-IV riboswitch

The *Clostridium botulinum* guanidine-IV riboswitch was investigated in this study. The secondary structures of the guanidine-IV riboswitch are depicted in **Figures 1A** and **1B**. In the absence of the guanidinium cation (Gua^+), the terminator consists of the aptamer domain (in black) and poly-U tail (in red). This terminator is proposed to terminate transcription by dissociating RNA polymerase from the transcription system (**Figure 1A**). However, in the presence of Gua^+, the formation of a KL (in green, **Figure 1B**) hinders the formation of the complete terminator stem. This leads to the formation of the anti-terminator conformation, and transcription of the full-length riboswitch comprises the extended nucleotides (in blue), in addition to the terminator/anti-terminator region (in red, **Figures 1B** and **1C**). Consequently, the anti-terminator conformation activates the expression of the downstream genes (**Figures 1C** and **1D**). In our study, we noted that the transcriptional read-through of the guanidine-IV riboswitch during the single-round PLOR reaction was sensitive to Gua^+, exhibiting an apparent EC50 value of 68.7 ± 7.3 μM (**Figure 1D**) (Chien et al., 2023). This is comparable to the reported K_D of approximately 64 μM that was determined by in-line probing (Salvail et al., 2020). Higher read-through efficiencies were detected at higher Gua^+ concentrations, consistent with previous findings (Lenkeit et al., 2020). In order to probe the structural changes of different domains in the guanidine-IV riboswitch under various conditions, we applied PLOR to introduce Cy3 and Cy5 at sites 78 and 35 in the aptamer (riboG-apt), terminator/anti-terminator (riboG-term), and full-length guanidine-IV riboswitch (riboG). Sites 78 and 35 are close to the KL, making them suitable for monitoring the KL formation at different Mg^{2+} and Gua^+ concentrations.

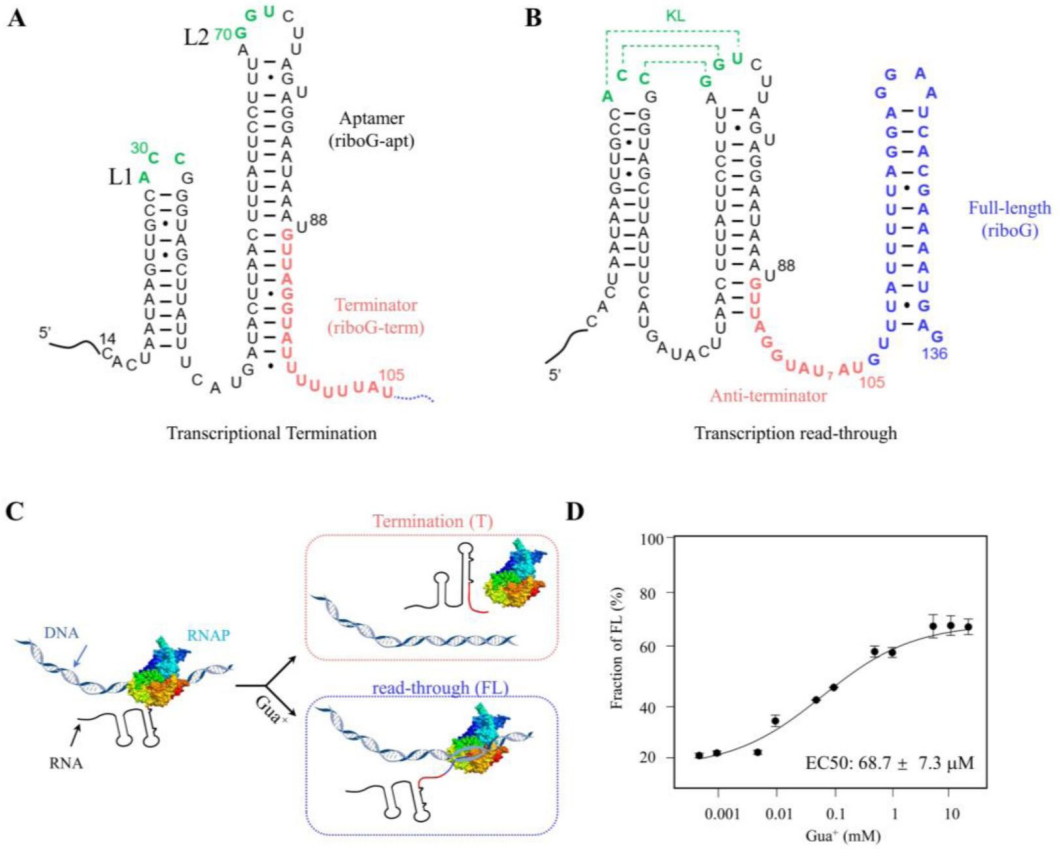

Figure 1.

Characteristics of the *C. botulinum* guanidine-IV riboswitch.

(A, B) The secondary structures of the transcriptional termination and read-through states of the guanidine-IV riboswitch. The full-length of the guanidine-IV riboswitch contains the aptamer domain (black), terminator (red) and the extended sequence (blue). The green nucleotides are involved in forming a KL in the anti-terminator state. (C) A transcriptional model of the guanidine-IV riboswitch. The DNA is shown in blue ribbons. The colors in the RNA are encoded as in (A) and (B). And the addition of Gua^+ facilitates transcription read-through. (D) The percentages of the transcription read-through plotted with 0.5 μM–20.0 mM Gua^+ at 6.0 mM Mg^{2+} in the three independent transcription termination reactions.

smFRET revealed the significant effects of Mg^{2+} and Gua^{+} on riboG-apt

smFRET is a powerful method that can detect multiple conformations by measuring the energy transfer efficiency (E_{FRET}) of a pair of fluorophores at the single molecule level. This technique has been extensively employed to investigate the conformational dynamics of RNA at the single-molecule level (Manz et al., 2017; Uhm et al., 2018). When the riboG-apt labeled with dual fluorophore-labeled (**Figure 2A**, **Figure 2**–figure supplement 1) was examined, a single peak (E_{FRET} ~ 0.2) was observed in the presence of 0 mM Mg^{2+} and 0 mM Gua^{+} (**Figure 2B**). This peak is believed to correspond to the unfolded structure of riboG-apt, where the KL is not formed and thus, the labeled sites are distant from each other. Furthermore, in the presence of 2.0 mM Mg^{2+}, three peaks (E_{FRET} ~ 0.2, 0.5, and 0.8) were observed, as revealed by hidden Markov modeling (**Figure 2C**). This suggests the coexistence of at least three structures when 2.0 mM Mg^{2+} is present, with the peak at an E_{FRET} of approximately 0.8 likely representing the KL formation. The peak characterized by an E_{FRET} ~ 0.5 emerged at varying collection rates and was indicative of a more compact conformation compared to the unfolded structure, which we referred to as the pre-folded structure (**Figure 2D**, **Figure 2**– figure supplement 2 and 3). Notably, at 2.0 mM Mg^{2+}, these three states exhibited high dynamics, with transitions occurring particularly between the pre-folded and the unfolded states (**Figures 2B**, 2C, **Figure 2**– figure supplement 2 and 3). Our results demonstrate that the presence of Mg^{2+} induces a conformational change in the unfolded riboG-apt, leading to the adoption of more compact pre-folded and folded conformations. The proportion of the folded conformation significantly increased to approximately 90% at 20.0 mM Mg^{2+} (**Figure 2E** and **Figure 2**– figure supplement 4G). At high concentrations of Mg^{2+}, riboG-apt remained flexible and dynamic in its transition between states (**Figure 2**– figure supplement 4). However, at a higher concentration of 50.0 mM Mg^{2+}, the proportion of the pre-folded and unfolded conformations were more prevalent at 50.0 mM Mg^{2+} than at 20.0 mM Mg^{2+}. This suggests that an excess of Mg^{2+} may promote the pre-folded and even unfolded conformations.

Gua^{+} also had the ability to promote the folded conformation (E_{FRET} ~ 0.8) of riboG-apt. However, Gua^{+} exhibited lower efficacy compared to Mg^{2+}, as evidenced by the proportion of the folded conformation being approximately 25% in the presence of 20.0 mM Gua^{+}. This value is significantly lower than the approximately 90% observed in the presence of 20.0 mM Mg^{2+} (**Figure 2E**, **Figure 2**– figure supplement 4G and 5F). Our observations also revealed that riboG-apt exhibited pronounced dynamics, frequently transiting among the three states at 10.0–100.0 mM Gua^{+} (**Figure 2**– figure supplement 5E–H). The presence of Mg^{2+} was critical in facilitating the induction of the folded state by Gua^{+}. Notably, riboG-apt showed increased susceptibility to Gua^{+} in the presence of Mg^{2+} (**Figure 2F**, **Figure 2**– figure supplement 6). Upon the addition of 0.5 mM Gua^{+} and 0.5 mM Mg^{2+}, the KL-folded conformation predominated in riboG-apt. The proportion of the KL-folded conformation increased to over 40%, which was comparable to the effect observed with a 20-fold increase in 0.5 mM Gua^{+} in the absence of Mg^{2+} (**Figure 2**– figure supplement 5B and 6E). Interestingly, at 0.5 mM Mg^{2+}, Gua^{+} bound to riboG-apt with a K_d of 286.0 ± 18.1 μM (**Figure 2**– figure supplement 6H), higher than the K_d of 64 μM that was determined by in-line probing in the presence of 20 mM Mg^{2+} (Salvail et al., 2020). This difference is likely due to the low concentration of Mg^{2+}, which has a weak ability to help guanidine induced the KL conformation. In addition, we observed that riboG-apt became more stable as the concentration of Gua^{+} increased, particularly in the presence of high Mg^{2+} (**Figure 2**– figure supplement 7). Surprisingly, the proportion of the folded conformation hardly increased when Mg^{2+} exceeded 2.0 mM in the presence of 1.0 mM Gua^{+}. Taking into account that Gua^{+} was present in a positively charged state in the buffer employed for our FRET studies, we conducted additional experiments to investigate the impact of commonly used cations, including Na^{+}, K^{+}, and urea (a structural analog of guanidine). Interestingly, we observed minimal changes in the folded conformation of riboG-apt upon the addition of Na^{+}, K^{+}, or urea. These findings suggest that the effects of Gua^{+} on

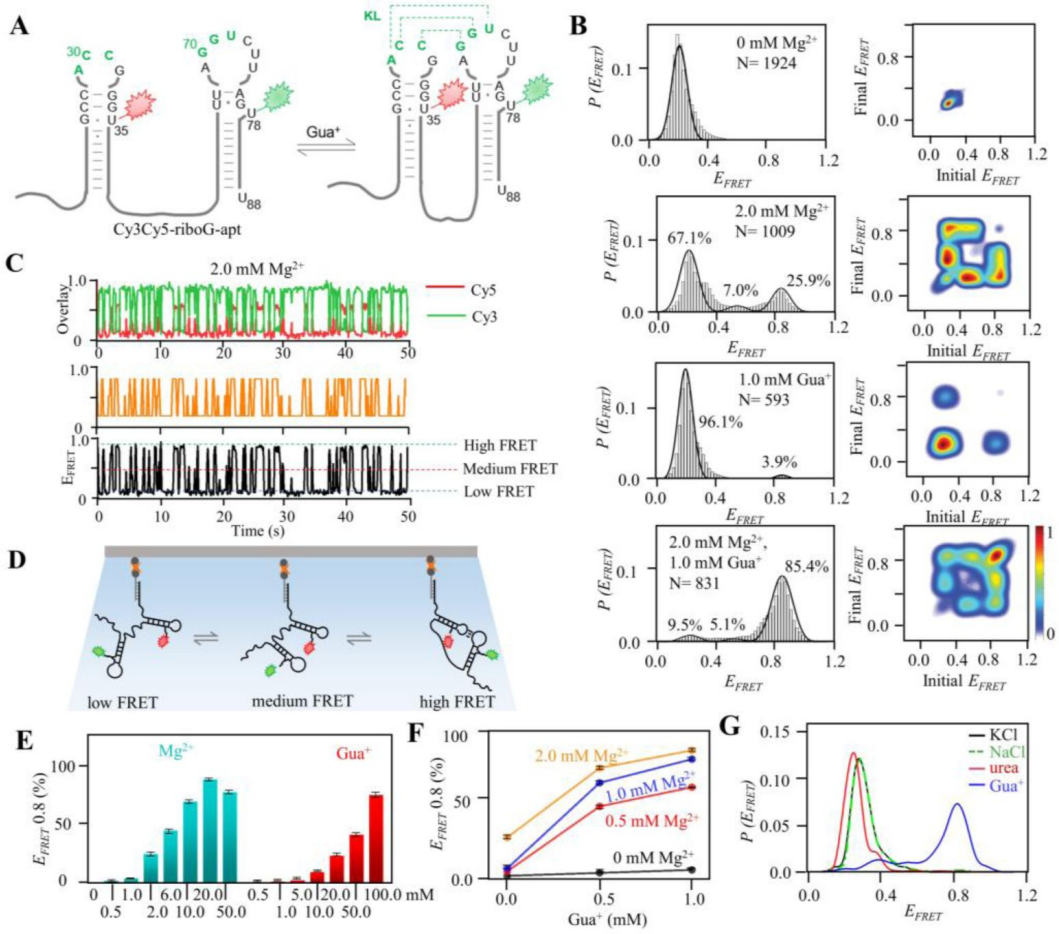

Figure 2.

smFRET studies of post-transcriptional Cy3Cy5-riboG-apt at different concentrations of Mg^{2+} and Gua^{+}.

(A) The secondary structures of Cy3Cy5-riboG-apt at the unfolded (left) and the folded state (right). Cy3 and Cy5 are shown by green and red sparkles, respectively. (B) smFRET histograms and transition density plots for Cy3Cy5-riboG-apt at 0 mM Mg^{2+}, at 2.0 mM Mg^{2+}, at 1.0 mM Gua^{+}, and at 2.0 mM Mg^{2+} and 1.0 mM Gua^{+}. (C) HMM analysis of smFRET time trace of Cy3Cy5-riboG-apt at 2.0 mM Mg^{2+}, the time resolution is 0.1s. (D) Schematic diagram for three conformations of Cy3Cy5-labeled RNA in smFRET experiments. The Cy3Cy5-labeled RNA is hybridized with a biotinylated DNA and immobilized on the slides. (E) The percentages of the folded conformation (E_{FRET} ~ 0.8) of Cy3Cy5-riboG-apt at 0–50.0 mM Mg^{2+} (cyan columns) and 0.5–100.0 mM Gua^{+} (red columns). (F) The percentages of the folded conformation of Cy3Cy5-riboG-apt change with Gua^{+} at 0, 0.5, 1.0 and 2.0 mM Mg^{2+}. (G) FRET histograms of Cy3Cy5-riboG-apt at 100.0 mM KCl (black curve), NaCl (green curve), urea (red curve) and guanidine (blue curve). The experiments were repeated for three times.

the folded conformation are distinct from those of the tested cations. Furthermore, our results indicate that Gua^+ specifically binds to riboG-apt and induces structural changes as a ligand, rather than simply acting as a general cation or chaotrope (**Figure 2G**).

The highly conserved nucleotides surrounding the KL are crucial for its formation (Lenkeit et al., 2020). To test our hypothesis that the state with E_{FRET} ~ 0.8 corresponds to the conformation with the KL, we preformed smFRET analysis on several mutations at these crucial nucleotides (**Figure 2** – figure supplement 8–10). Consistent with our expectations, the peaks with E_{FRET} ~ 0.8 was significantly diminished in the riboG-G71C mutant, which features a single nucleotide mutation at site 71 (with 97% nucleotide conservation) in the KL (**Figure 2** – figure supplement 8A and 8B). It is worth noting that the C30G and G71C mutant, which were initially expected to restore a base pair in the KL, did not successfully bring about the anticipated peak of E_{FRET} ~ 0.8 (**Figure 2** – figure supplement 8C and 8D). On the other hand, the riboG-U72C mutant exhibited a lower proportion at the state with E_{FRET} ~ 0.8 than riboG-apt. However, the A29G and U72C mutations restored a base pair in the KL, as well as the formation of the KL (**Figure 2** – figure supplement 9). Furthermore, our investigation revealed that the G77C mutant, involving a single nucleotide mutation at a highly conversed site, 77 (with 97% nucleotide conservation), also hindered the formation of the KL (**Figure 2** – figure supplement 10). This finding aligns with previous research (Lenkeit et al., 2020) and the predicted second structure of G77C mutation by Mfold (Zuker, 2003).

smFRET analysis revealed the slight effects of Mg^{2+} and Gua^+ on riboG-term and full-length riboG

Unlike riboG-apt, riboG-term labeled with dual fluorophores exhibited the coexistence of three conformations, characterized by E_{FRET} values of approximately 0.2, 0.5, and 0.8 (**Figure 3A**, **Figure 3**–figure supplement 1–5). This coexistence was observed even in the absence of Mg^{2+} and Gua^+ (**Figure 3B**, **Figure 3**–figure supplement 2A and 2B). This indicates that monovalent ions in the buffer can facilitate the formation of stable guanidine-IV riboswitch. The sensitivity of RiboG-term to Gua^+ was significantly lower compared to riboG-apt. This is evidenced by the fact that, in the presence of 2.0 mM Mg^{2+}, the addition of 1.0 mM Gua^+ only resulted in an increase of approximately 4% the folded conformation for riboG-term, while it was approximately 60% for riboG-apt (**Figures 2B** and **3B**). With the increase of either Mg^{2+} from 0 to 50.0 mM or Gua^+ from 0 to 100.0 mM, less than 12% of the molecules transited dynamically among the three states of riboG-term (**Figure 3**–figure supplement 2 and 3). This finding suggests that the unfolded structure of riboG-term without the KL (E_{FRET} ~ 0.2) is stable, and high concentrations of Mg^{2+} or Gua^+ only slightly affect the KL formation (**Figure 3C**). In the presence of 0.5 mM Mg^{2+}, the structural change of riboG-term in response to increasing Gua^+ was negligible (**Figure 3D**, **Figure 3**–figure supplement 4). Surprisingly, in the presence of 1.0 mM Gua^+, the conformation dynamics of riboG-term became more evident as Mg^{2+} increased. Moreover, at high Mg^{2+} concentrations, such as 10.0 mM, the abundance of the folded conformation (E_{FRET} ~ 0.8) significantly elevated with increasing Gua^+ (**Figure 3E** and **Figure 3**–figure supplement 5). This suggests that Gua^+ enhances the flexibility of riboG-term, potentially triggering its structural changes and facilitating the regulatory function of riboG in the presence of Mg^{2+}. In contrast to riboG-term, both its G71C and C30G-G71C mutants displayed a reduced proportion of the state with E_{FRET} ~ 0.8. Remarkably, the fractions of E_{FRET} ~ 0.8 remained unaffected by the addition of 1.0 mM Gua^+ in these mutants. Distinct from riboG-term, no structural transitions between states were observed in the two mutants (**Figure 3** – figure supplement 6). Regarding the U72C mutant of riboG-term, the mutation at the site 72 had a reduced impact on the KL conformation in the presence of 1.0 mM Gua^+ and 2.0 mM Mg^{2+}. However, the increased proportion of E_{FRET} ~ 0.8 in the A29G-U72C mutant of riboG-term suggests that these mutations can restore the base-pairing between sites 29 and 72, as well as facilitate the formation of the KL (**Figure 3** – figure supplement 7).

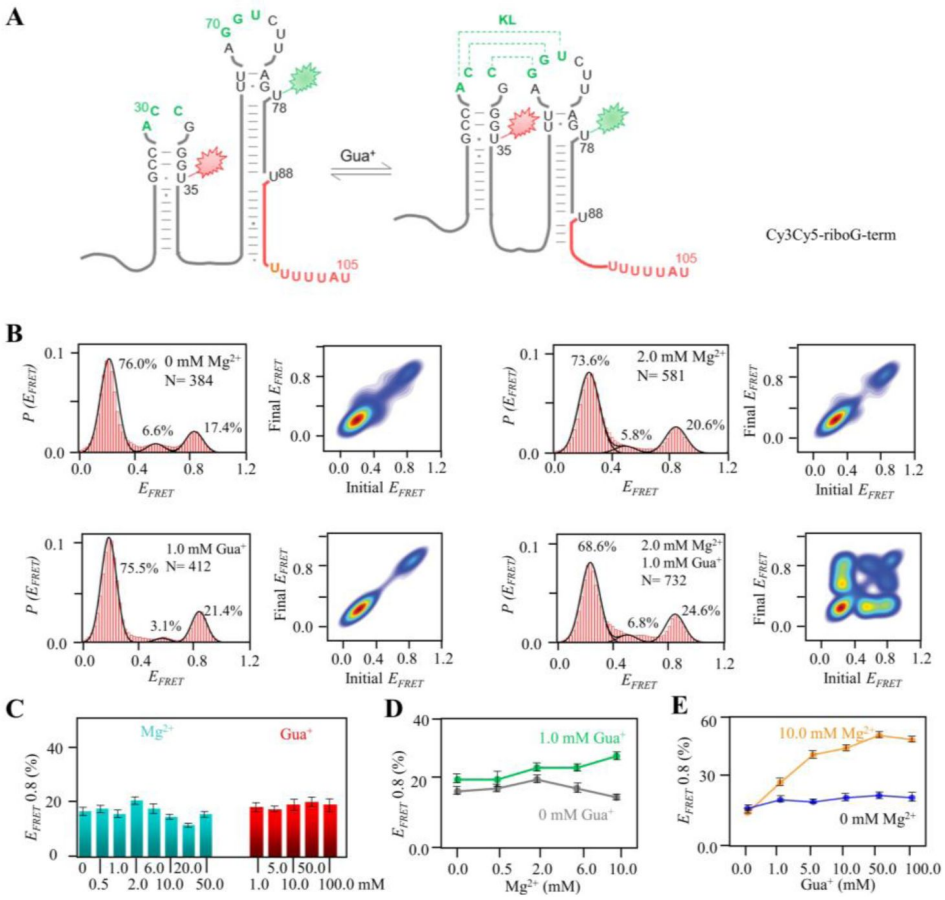

Figure 3.

smFRET studies of post-transcriptional riboG-term at different concentrations of Mg^{2+} and Gua^{+}.

(A) The secondary structures of Cy3Cy5-riboG-term at the unfolded (left) and the folded state (right). (B) smFRET histograms and transition density plots of Cy3Cy5-riboG-term at 0 mM Mg^{2+}, at 2.0 mM Mg^{2+}, at 1.0 mM Gua^{+}, and at 2.0 mM Mg^{2+} and 1.0 mM Gua^{+}. (C) The percentages of the folded conformation (E_{FRET} ~ 0.8) of Cy3Cy5-riboG-term at 0–50.0 mM Mg^{2+} (cyan columns) and 1–100.0 mM Gua^{+} (red columns). (D) The percentages of the folded conformation of Cy3Cy5-riboG-term change with Mg^{2+} at 0 (black) and 1.0 mM Gua^{+} (green). (E) The percentages of the folded conformation of Cy3Cy5-riboG-term change with Gua^{+} at 0 (blue) and 10.0 mM Mg^{2+} (orange).

In the presence of Mg^{2+} and/or Gua^{+}, the FRET histogram of full-length riboG (**Figures 4A** and **Figure 4**–figure supplement 1) displayed a greater number of peaks compared to riboG-apt and riboG-term (**Figures 4B** and **Figure 4**–figure supplement 2). Additionally, the smFRET traces revealed structural transitions among the states, as shown in **Figure 4**–figure supplement 2–5. The presence of more structures in the full-length riboswitch compared to the aptamer domain is consistent with findings in other RNA molecules, such as the 2'-dG riboswitch (Helmling et al., 2017). Notably, upon the addition of 1.0 mM Gua^{+} in the presence of 2.0 mM Mg^{2+}, the proportion of the new peak (E_{FRET} ~ 0.4) increased from 19% to 29%, and then decreased as the Mg^{2+} concentrations increased from 2.0 to 10.0 mM (**Figure 4**–figure supplement 2D and 4B–D). In the absence of Gua^{+}, the addition of 0–50.0 mM Mg^{2+} only slightly altered the proportion of the folded conformation (E_{FRET} ~ 0.8) of the full-length riboG (**Figure 4**–figure supplement 2). Even in the presence of 1.0 mM Gua^{+}, an increase in Mg^{2+} concentration from 0 to 10.0 mM had a slight effect on the proportion of the folded conformation (**Figure 4**–figure supplement 4B–D). However, the effect of Gua^{+} on full-length riboG in the presence of 10.0 mM Mg^{2+} was significantly more pronounced compared to its effect in the absence of Mg^{2+} (**Figure 4C** and **Figure 4**–figure supplement 5B–F). The impact of Mg^{2+} and Gua^{+} on the folded conformation of full-length riboG showed similarities to their effects on riboG-term but had distinct differences compared to their effects on riboG-apt (**Figures 4D** and **4E**). Overall, the effects of Mg^{2+} and Gua^{+} on the structures of full-length riboG and riboG-term were weaker compared to their effects on riboG-apt. Upon comparing the G71C and C30G-G71C mutants of the full-length riboG with their wild-type counterpart, it was observed that the wild-type adopted higher proportions of the state with E_{FRET} ~ 0.8 (**Figure 4**– figure supplement 6). Regarding the U72C and A29G-U72C mutants of the full-length riboG, their behaviors with regards to the peak with E_{FRET} ~ 0.8 were similar to that of their counterparts in riboG-term (**Figure 4**– figure supplement 7).

Kinetic analysis of smFRET data to identify the folding pathway of the guanidine-IV riboswitch

The guanidine-IV riboswitch exhibits dynamic behavior, with its structural transitions in response to Mg^{2+} and Gua^{+} closely linked to transcription termination. The relative free energy ($\Delta\Delta G$) was calculated based on the state populations in the FRET histogram (**Figures 5A** and **5B**). For riboG-apt, both the pre-folded and folded states displayed higher $\Delta\Delta G$ values compared to the unfolded state, indicating that the former states were less stable in the presence of 2.0 mM Mg^{2+}. However, the addition of 1.0 mM Gua^{+} successfully reduced the $\Delta\Delta G$ of the folded state to a level lower than that of the unfolded state (**Figure 5A**). Meanwhile, only slight decreases in $\Delta\Delta G$ were observed for riboG-term and riboG upon the addition of 1.0 mM Gua^{+} in the presence of 2.0 mM Mg^{2+} (**Figure 5B**). The dwell time distributions were obtained from the single-molecule trajectories of FRET data for riboG-apt, riboG-term, and riboG (**Figures 5C–E** and **Figure 5**–figure supplement 1–4). The exponential decays of the dwell time were fitted to a first-order kinetic equation, allowing for the determination of dwell time and rate constants for the individual states of riboG-apt (**Figures 5C–E**). Based on these results, we proposed folding pathways to illustrate the transcriptional fate of the guanidine-IV riboswitch under different conditions (**Figure 5F** and **Figure 5**–figure supplement 4). The analysis of the dwell time data from single-molecule trajectories indicated that the folding process of riboG-apt was influenced by Mg^{2+} and/or Gua^{+}. In the presence of 2.0 mM Mg^{2+}, there was inefficient structural switching from the unfolded riboG-apt (τ ~ 0.69 s) to the pre-folded state (τ ~ 0.11 s) or folded riboG-apt (τ ~ 0.40 s), resulting in the production of the terminator during transcription (red arrows, **Figure 5F**). Conversely, in the presence of 1.0 mM Gua^{+}, the primary switching of riboG-apt occurred between the unfolded (τ ~ 0.60 s) and folded states (τ ~ 1.04 s), which can subsequently be transcribed into the anti-terminator (blue arrows, **Figure 5F**).

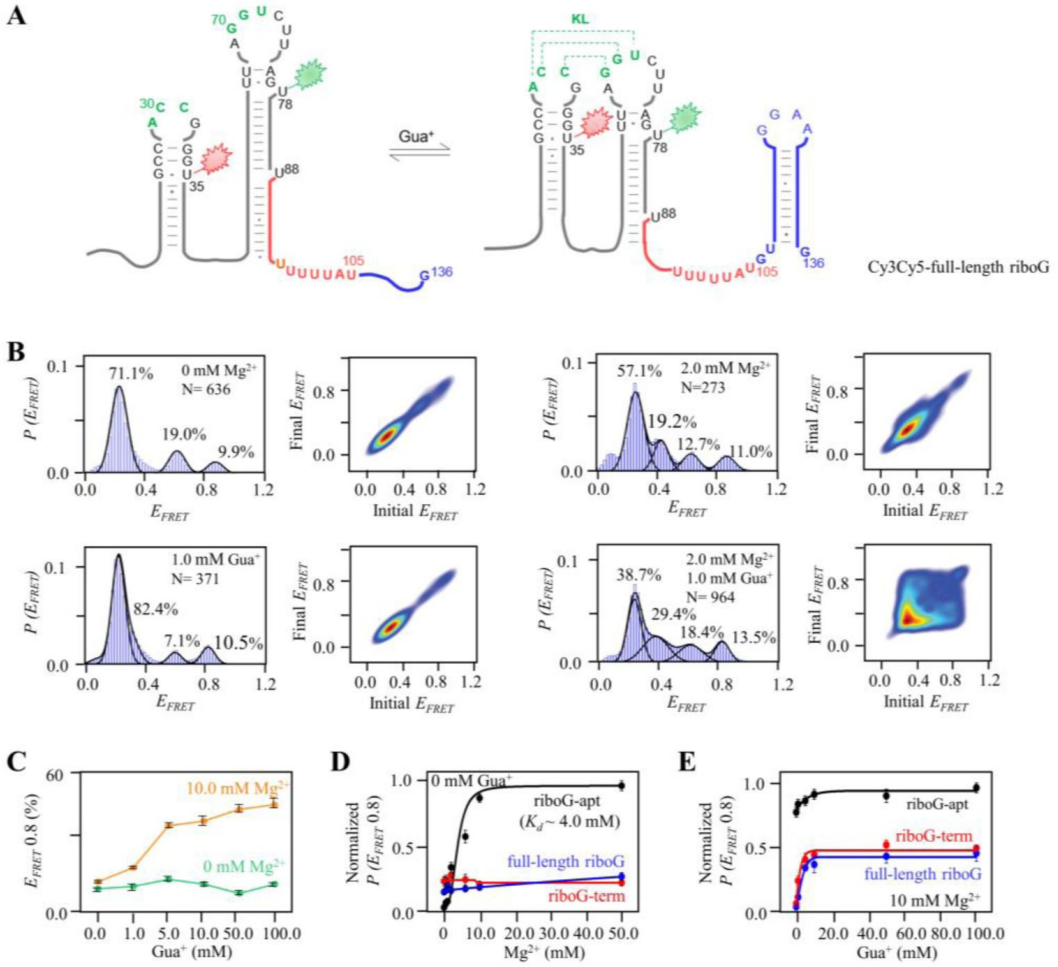

Figure 4.

smFRET studies of the isolated full-length riboG at different concentrations of Mg^{2+} and Gua^{+}.

(A) The secondary structures of Cy3Cy5-ful-length riboG at the unfolded (left) and the folded state (right). The full-length riboG contains the aptamer domain (black), terminator (red) and the extended sequence (blue). Cy3 and Cy5 are shown by green and red sparkles, respectively. (B) smFRET histograms and transition density plots for Cy3Cy5-full-length riboG at 0 mM Mg^{2+}, at 2.0 mM Mg^{2+}, at 1.0 mM Gua^{+}, and at 2.0 mM Mg^{2+} and 1.0 mM Gua^{+}. (C) The percentages of the folded conformation of Cy3Cy5-full-length riboG change with Gua^{+} at 0 (green) and 10.0 mM Mg^{2+} (orange). (D–E) The normalized percentages of the folded conformation of Cy3Cy5-riboG-apt (black), Cy3Cy5-riboG-term (red) and Cy3Cy5-full-length riboG (blue) at 0–50 mM Mg^{2+} (D) and 0–100.0 mM Gua^{+} in the presence of 10.0 mM Mg^{2+} (E).

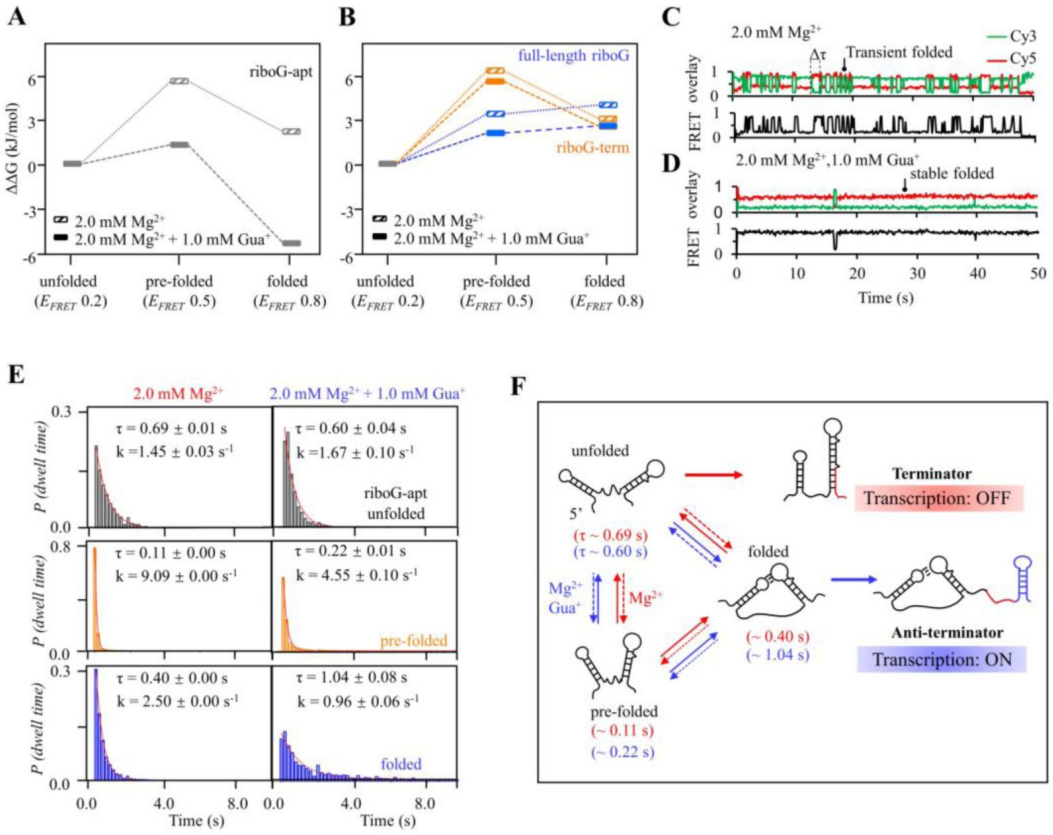

Figure 5.

Relative free energy (*ΔΔG*) and kinetics analysis of isolated riboG-apt, riboG-term and full-length riboG.

(A) The relative free energy of the pre-folded and folded states of riboG-apt in the presence of 0 and 1.0 mM Gua^+ at 2.0 mM Mg^{2+}. The free energy of the unfolded state was referred as control. (B) The relative free energy of the pre-folded and folded states of riboG-term (orange) and full-length riboG (blue) in the presence of 0 and 1.0 mM Gua^+ at 2.0 mM Mg^{2+}. (C–D) Representative time traces of riboG-apt at 0 (C) and 1.0 mM Gua^+ (D) in the presence of 2.0 mM Mg^{2+}. Δτ is the dwell time. (E) The lifetime (τ) and rate constant (k) of unfolded (black), pre-folded (orange) and folded (blue) states of riboG-apt was determined by exponential decays of the dwell time distributions. (F) Schematic diagram of riboG-apt folding and transcriptional processes at 2.0 mM Mg^{2+} in the presence of 0 mM Gua^+ (red) and 1.0 mM Gua^+ (blue).

smFRET analysis revealed the Gua^+-sensitive transcription window of riboG

The sensitivity of Gua^+ varied among the post-transcriptional riboG-apt, riboG-term, and full-length riboG sequences. The folding and interactions of RNA during transcription play a critical role in its control functions for transcriptional riboswitch. To mimic how nascent riboG responds to Gua^+ and its regulatory effects during transcription, we utilized PLOR to control its transcription at a single-nucleotide pace. Simultaneously, we collected smFRET data from active transcription elongation complexes (ECs) containing nascent RNA of different lengths (**Figures 6A**, 6B and **Figure 6**–figure supplement 1). PLOR is a liquid–solid hybrid phase transcription process that allows for pausing transcription at specific positions by omitting certain nucleotide triphosphates (NTPs). This paused transcription can then be restarted by adding the necessary NTPs. This unique "pause–restart" transcriptional mode enables the evaluation of instant changes in the environment, such as the addition or removal of Gua^+ at specific steps, facilitating the monitoring of nascent RNA under varied conditions. To investigate the range of ligand-responsiveness in riboG, we employed PLOR to generate various transcriptional complexes with different RNA length, this allowed us to assess the impact of Gua^+ on the guanidine-IV riboswitch throughout the transcription process. We monitored the behavior of active transcription complexes containing guanidine-IV riboswitches with varying lengths of 87 to 105 nucleotides (nt) using smFRET (**Figures 6C–I** and **Figure 6**–figure supplement 2–5). To distinguish between the different complexes, we named them based on their nucleotide length, for example, the EC-87 for the 87 nt complex. We collected smFRET histograms for EC-87, EC-88, EC-89, EC-91, EC-94, EC-96, and EC-105 in the presence of 0.5 mM Mg^{2+} and either 0 or 10.0 mM Gua^+ (**Figures 6C–I** and **Figure 6**–figure supplement 2–3). Three distinct peaks (E_{FRET} ~ 0.2, 0.5, and 0.8) were observed, with the high-FRET peak suggesting the presence of a newly folded RNA structure, potentially containing a KL, as the transcript size exceeded 87 nt. In the presence of 0.5 mM Mg^{2+}, the proportion of the folded structure slightly decreased during transcription from 87 to 88 nt (from approximately 15% to 13%), but then sharply decreased to 3% at 89 nt. The addition of Gua^+ significantly increased the proportion of the folded state for EC-88 compared to EC-87. For longer ECs, such as EC-89, EC-91, and EC-94, the proportion of the folded state remained relatively stable (**Figures 6E–I**, **Figure 6**–figure supplement 2-3). At 0.5 and 2.0 mM Mg^{2+}, the proportions of the peaks changed differently, but EC-88 exhibited more dramatic changes than other ECs upon the addition of Gua^+ (**Figure 6J** and **Figure 6**– figure supplement 2–5). These results suggest that the optimal formation of KL occurs during transcription of the 88 nt nascent RNA, and a drastic structural switch takes place between 88 and 89 nt in the presence of Mg^{2+}. Interestingly, the addition of 1.0 mM Gua^+ induced more pronounced changes in the majority of ECs at higher Mg^{2+} concentrations (**Figure 6J** and **Figure 6**–figure supplement 4–5). These findings suggest that the ECs exhibit a greater propensity for structural transitions upon the addition of Gua^+ at high Mg^{2+} concentrations. Furthermore, under conditions of 0.5 mM Mg^{2+} and 10.0 mM Gua^+, the proportions of folded structures (E_{FRET} ~ 0.8) in EC-88 and EC-105 were approximately 36% and 14% lower, respectively, compared to those observed in the isolated post-transcriptional riboG-apt and riboG-term (**Figures 6D**, 6I, **Figure 2**–figure supplement 6G and **Figure 3**–figure supplement 4F). The T7 RNA polymerase (RNAP) sequestered about 8 nt of the nascent RNA, preventing the EC-88 construct from forming the P2 stem (Durniak et al., 2008; Huang & Sousa, 2000; Lubkowska et al., 2011; Tahirov et al., 2002; Wang et al., 2022; Yin & Steitz, 2002). Consequently, a pseudoknot structure potentially formed instead of the expected KL. This distinction may account for the observed heterogeneity between EC-88 and riboG-apt.

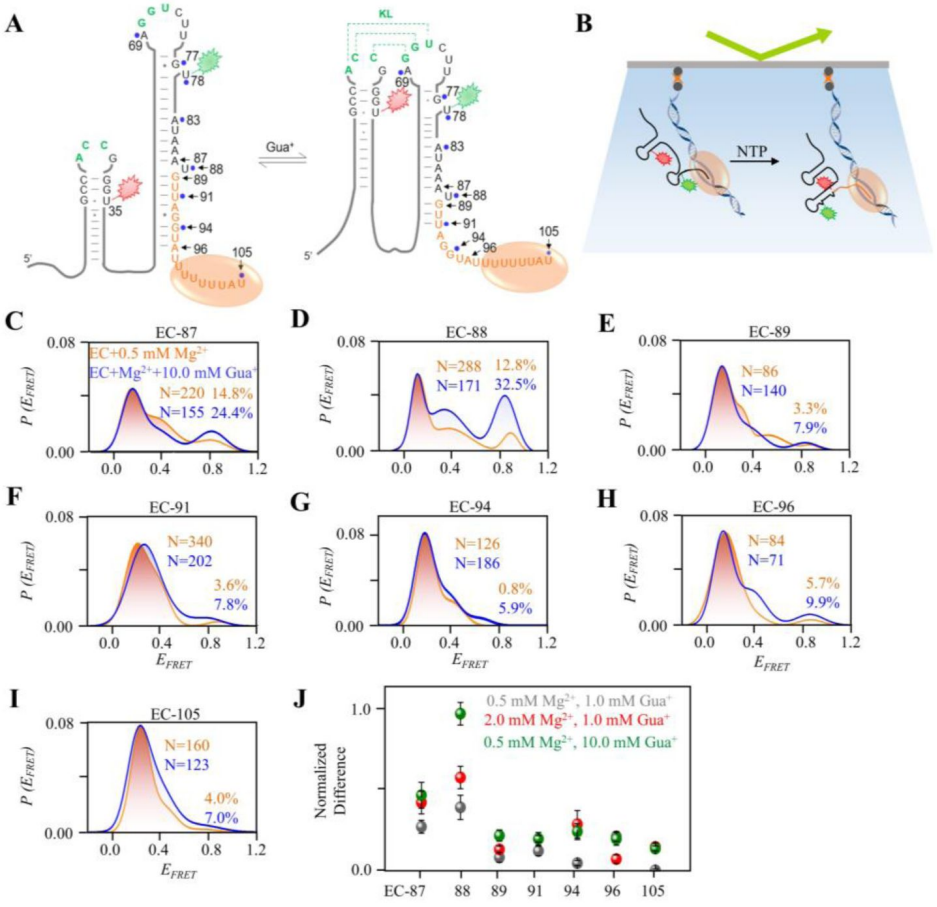

Figure 6.

smFRET studies of nascent riboG in ECs without and with Gua^+ at 0.5 mM Mg^{2+}.

(A) The ECs containing an RNA at the unfolded state (left) and the folded state (right). The pause sites of EC-87 to EC-105 are marked by black arrows, and the orange ellipse represents the T7 RNA polymerase. (B) Schematic diagram for smFRET experiment for ECs. The ECs were immobilized on the slides by their biotinylated DNA templates. (C–I) smFRET histograms for the EC-87 to EC-105 at 0 mM (orange) and 10.0 mM Gua^+ (blue) at 0.5 mM Mg^{2+}. (J) The normalized increase of the folded conformation (E_{FRET} ~ 0.8) of ECs upon the addition of 1.0 mM Gua^+ at 0.5 mM Mg^{2+} (grey), 10.0 mM Gua^+ at 0.5 mM Mg^{2+} (green) and 1.0 mM Gua^+ at 2.0 mM Mg^{2+} (red).

Gua^+ modulated the transcription of the guanidine-IV riboswitch at specific sequences

To investigate the regulatory functions of the nascent riboswitch at different lengths during transcription, we performed a transcriptional termination assay of the guanidine-IV riboswitch using PLOR (**Figure 7A** and **Figure 7**–figure supplement 1). Specifically, we carefully designed eight PLOR experiments to temporarily pause the transcription at nucleotides 69, 77, 78, 83, 88, 91, 94 and 105, respectively, before transcribing the remaining RNA fragment in the last step, following strategies 1–8 (**Figures 7B**, **Figure 7**–figure supplement 1B and 1C). In the absence of Gua^+, there was minimal change in transcriptional termination among strategies 1–7, but a sharp decrease of approximately 20% was observed for strategy 8 (**Figures 7C** and **7D**). However, with the addition of Gua^+ in the last step, there was little variation in transcriptional read-through of the guanidine-IV riboswitch among strategies 1–5, but a dramatic decrease in anti-termination from strategy 6 to strategy 8 (**Figures 7C** and **7D**). The detailed procedures of strategies 1-8 were shown in **Figure 7**– figure supplement 1. Furthermore, we observed a significant increase in read-through upon the addition of Gua^+ in our single-round transcription reactions when the RNA length reached 88 nt (**Figure 7**–figure supplement 1D). Additionally, a slight increase in read-through was observed at the pausing site 105, which is consistent with the smFRET data presented in **Figure 6J**. This indicates that Gua^+ can still bind and induce slight structural changes in the guanidine-IV riboswitch, even if its full terminator sequence has been transcribed. Our findings from *in vitro* transcriptional termination assays and smFRET results, indicating that EC-91 exhibits a more stable fold with a longer stem, making it less sensitive to environmental changes compared to EC-88 (**Figures 6F** and **Figure 7**–figure supplement 1D).

Discussion

The guanidine-IV riboswitch exhibits similarities to the guanidine-I riboswitch in gene regulatory mechanism, functioning as a transcriptional riboswitch. Structurally, it resembles the guanidine-II riboswitch through the formation of loop-loop interactions upon binding to guanidine (Battaglia & Ke, 2018; L. Huang et al., 2017; Lin Huang et al., 2017; Lenkeit et al., 2020; Nelson et al., 2017; Reiss & Strobel, 2017; Salvail et al., 2020). In this study, we have demonstrated that both Mg^{2+} and Gua^+ play critical roles in promoting structural folding and transcriptional anti-termination in the guanidine-IV riboswitch. Based on our findings, we propose a model illustrating the termination/anti-termination process of the guanidine-IV riboswitch as transcription progresses (**Figure 8**). In the presence of Mg^{2+}, the proportion of the anti-terminator induced by Gua^+ increases as transcription progresses up to EC-88.

However, after EC-88, a significant decrease is observed up to EC-105. The elongation of transcription from EC-88 to EC-105 leads to impaired pseudoknot or KL formation and an increase in terminator abundance. This incremental switch from the anti-terminator to the terminator from EC-88 to EC-105 is influenced by the elongating P2 structure (**Figure 8**). The competition between the P2 and KL structures determines the proportions of the terminator and the anti-terminator in the guanidine-IV riboswitch. The stability of the terminator is enhanced by the presence of P2, and the increase in base pairs within P2 strengthens the terminator as transcription proceeds. On the other hand, the stability of the anti-terminator is dependent on the formation of pseudoknot or KL. The elongation of P2 shortens the flexible linker between P1 and P2, which creates steric hindrance for KL after EC-88. Furthermore, the addition of Gua^+ facilitates the functional switch from the terminator to the anti-terminator for constructs ranging from EC-87 to EC-105. Here we propose a narrow Gua^+-sensitive transcription window for the guanidine-IV

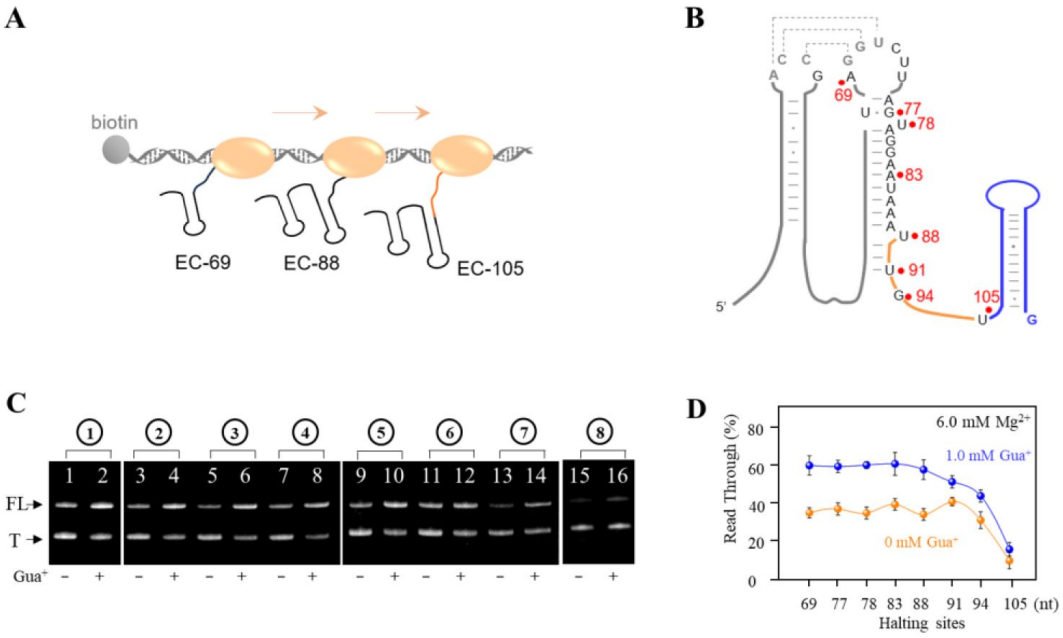

Figure 7.

Ligand-mediated conformational switching of riboG during transcription.

(A) The schematic diagram of synthesizing ECs with nascent RNAs by *in vitro* transcriptional pause using PLOR reactions. The orange ellipse represents T7 RNA polymerase. (B) The secondary structures of full-length riboG. The halting sites of EC-69, EC-77, EC-78, EC-83, EC-88, EC-91, EC-94 and EC-105 are marked by red dots. C, PAGE images of the crude products collected at the last step of individual PLOR strategy in the absence and presence of 1.0 mM Gua^+. FL and T are represented for the read-through and terminated RNA. The detail strategies were depicted in **Figure 7** –figure supplement 1B. D, The transcriptional read-through fractions were plotted with the last halting sites in 9 step-, 11 step-, 12 step-, 13 step-, 14 step-, 15 step-, 16 step- and 17 step-PLOR. The orange and blue curves are in the absence and presence of 1.0 mM Gua^+. Taking into consideration that the 17 step-PLOR reaction exhibited a pause within the terminator region, resulting in a significant amount of terminated product at step 16, crude products from steps 16 and 17 were collected for (C) and (D) of the 17 step-PLOR reaction (Lanes 15 and 16 in C).

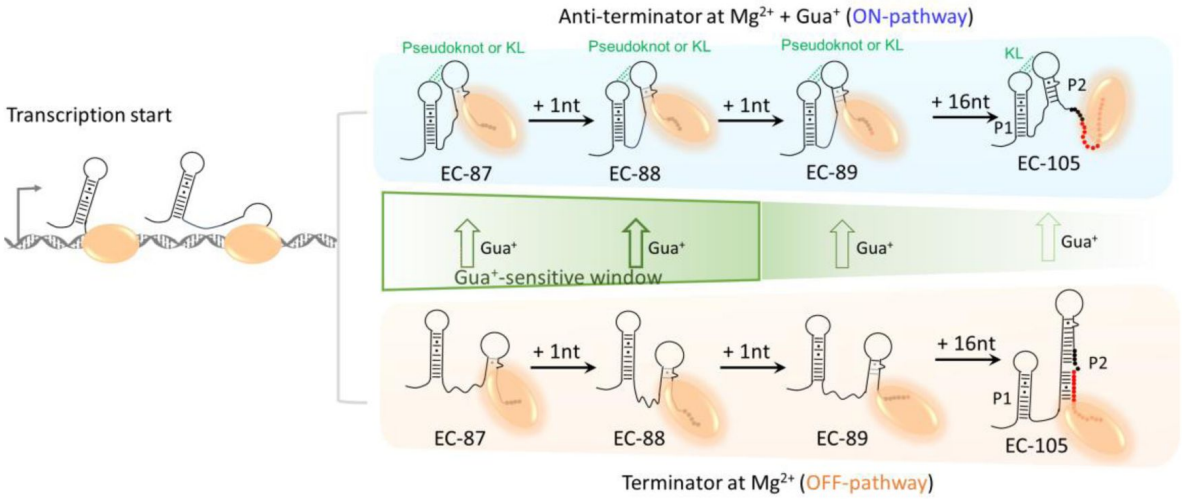

Figure 8.

Folding model of RiboG in the absence and presence of guanidine.

The folding pathways of anti-terminator conformation in the presence of Gua^+ and terminator conformation in the absence of Gua^+ are highlighted in blue and orange, respectively. The H-bonds in the KL are shown as dotted green lines. The nucleotides from EC-87 to EC-88 are shown as black dots, the nucleotides in termination sequence are shown as red dots in EC-89 and EC-105, and DNA templates from EC-87 to EC-105 are not displayed in the model. The T7 RNAP is shown as orange ellipse. The DNA templates are shown as gray ribbons. Green arrows represent the direction of structural switching in native riboG upon the addition of the Gua^+. The thicker the green arrow, the higher the switching percentages. And the Gua^+-sensitive transcription window of riboG from EC-87 to EC-88 is boxed by green lines.

riboswitch, with a dramatic switch observed during the extension from EC-87 to EC-88 upon Gua^+ addition (shown in a green box, **Figure 8**). It is worth noting that the ligand-sensitive sequence for the guanidine-IV riboswitch is located within the aptamer domain, spanning 88 nucleotides.

Our findings demonstrate that the guanidine-IV riboswitch possesses a distinct binding window that can be modulated by guanidine. The mechanism of anti-termination supports a model in which the formation of a long-range KL prevents the assembly of a rigid terminator. This distinguishes the guanidine-IV riboswitch from typical transcriptional riboswitches that rely on overlapping sequences and base-pair rearrangements for functional change (Strobel et al., 2019; Yadav et al., 2022; Zhao et al., 2017). Moreover, our results reveal the existence of at least three distinct states in the guanidine-IV riboswitch, including a folded state characterized by the presence of a KL that plays a critical role in ligand binding and transcriptional regulation. Importantly, the formation of the long-range KL in the aptamer domain is specifically responsive to guanidine, as other cations such as K^+, Na^+, and urea do not produce the same effect. While guanidine contributes to structural switching in the aptamer domain, its impact on the terminator or full-length guanidine-IV riboswitch is comparatively weak. Additionally, our data indicate that guanidine induces less significant changes once the RNA polymerase has transcribed the aptamer domain. It is worth noting that the RNAP utilized in our study is T7 RNAP, which exhibits distinct characteristics compared to bacterial RNAP in terms of transcriptional speed, dynamics, and interactions. However, Xue et al. have reported similarities between T7 and *E. coli* RNAP in the folding of nascent RNA. Additionally, Lou and Woodson have provided valuable insights into the co-transcriptional folding of the *glmS* ribozyme using T7 RNAP (Xue et al., 2023; Lou & Woodson, 2024).

In the transcriptional mimicking assay, the nascent RNA displayed a weaker response to guanidine compared to the post-transcriptional counterparts. The guanidine sensitivity of EC-87 indicates that guanidine regulation for the guanidine-IV riboswitch occurs before transcription of the aptamer domain is completed. Additionally, the sensitivity to guanidine gradually increases in the RNA within ECs until EC-88, after which it decreases. In other words, there exhibits a limited transcriptional window for the guanidine-IV riboswitch to dynamically respond to guanidine, and the inclination to form the terminator increases after transcribing 88 nucleotides, resulting in a decrease in the abundance of the KL-folded conformation. This aligns with previous findings that the transcription decision of a transcriptional riboswitch is made prior to terminator formation (Sherwood & Henkin, 2016; Wickiser et al., 2005). Nevertheless, the ligand-sensitive windows of riboswitches during transcription vary. In a study conducted by Helmling et al. using NMR spectroscopy, they proposed a broad transcriptional window for deoxyguanosine-sensing riboswitches, whereby the ligand binding capability gradually diminishes over several nucleotide lengths (Helmling et al., 2017). However, more recent research by Binas et al. and Landgraf et al. on riboswitches sensing ZMP, c-di-GMP, and c-GAMP revealed a narrow window with a sharp transition in binding capability, even with transcript lengths differing by only one or three nucleotides (Binas et al., 2020; Landgraf et al., 2022). In line with the findings for the c-GAMP-sensing riboswitch, our study on the guanidine-IV riboswitch also demonstrated a sharp transition in binding capability with just a single nucleotide extension. Our data also suggest that guanidine can induce slight structural changes in the guanidine-IV riboswitch even after the terminator domain has been transcribed and stabilized. Similar observations have been reported for other riboswitches, although the transcriptional window sensitive to the ligand differs among riboswitches (Wickiser et al., 2005).

Material and methods

DNA template preparation

The biotin labeled DNA templates were prepared by PCR as described earlier (Liu et al., 2018; Liu et al., 2015). The sequences of the DNA templates are listed in Supplementary Table S1. The primers used in PCR were ordered from Sangon Biotech (Shanghai, China). The DNA products generated from PCR were purified by 12% denaturing PAGE (polyacrylamide electrophoresis) before immobilized on streptavidin-coated agarose beads (Smart-Life Science, Changzhou, China) in the buffer (40 mM Tris-HCl, 100 mM K_2SO_4, 6 mM $MgSO_4$, pH 8.0) as described earlier (Liu et al., 2018). The solid-phase DNA templates were stored at 4 °C before usage.

Cy3Cy5-labeled riboG-apt, riboG-term and full-length riboG synthesis

The Cy3Cy5-labeled RNA used in smFRET were synthesized by PLOR as described earlier (Liu et al., 2018; Liu et al., 2015), and RNA sequences were depicted in Supplementary Tables S1 and S2. The schemes and reagents of synthesis of Cy3Cy5-riboG-apt, Cy3Cy5-riboG-term and Cy3Cy5-full-length riboG are listed in Supplementary Tables S3, S4 and S5. For Cy3Cy5-riboG-apt synthesis, 10 μM DNA-beads gently shook with 10 μM T7 RNAP, 0.96 mM ATP, 0.96 mM GTP and 96 μM UTP in the buffer (40 mM Tris-HCl, 100 mM K_2SO_4, 6 mM $MgSO_4$, 10 mM DTT, pH 8.0) at 37 °C for 15 min in the first step. The reaction mixture was filtered by solid-phase extraction and rinsed for 3~4 times in the buffer (40 mM Tris-HCl, 6 mM $MgSO_4$, pH 8.0). And the bead-rinsing procedure was performed before the addition of NTPs in each step except noted. The residual steps were proceeded in the elongation buffer (40 mM Tris-HCl, 6 mM $MgSO_4$, 10 mM DTT, pH 8.0) at 25 °C for 10 min with the addition of different NTP mixture at individual step as listed in Supplementary Table S3. The Cy3Cy5-labeled riboG-apt was collected at the last step, purified by 12% denaturing PAGE and reversed phase HPLC loaded with C8 column (4.6*250 mm, Cat. No. EXL-122-2546U, Phenomenex Luna, USA) as described earlier. The Cy3Cy5-riboG-term and Cy3Cy5-full-length riboG were synthesized as Cy3Cy5-riboG-apt except different NTPs were added. The purified RNA was stored at -80 °C before usage. T7 RNAP was utilized in the PLOR and *in vitro* transcription reactions except noted.

Preparation of transcription complexes containing RNA at different lengths

The RNA sequences in the transcription complexes (ECs) are listed in Supplementary Table S6, and the ECs were collected at different steps of PLOR as listed in Supplementary Table S7. For example, EC-87 was obtained as the following procedures: took 10 μL 10 μM DNA-beads from 200 μL of the PLOR reaction at step 14 and incubated with 1 μL 1 mM biotin at 25 °C for 20 min. The addition of biotin was to displace the biotin-labeled DNA template on the streptavidin-labeled beads, filtered by solid-phase exchange and collected the elution containing EC-87. EC-88, 89, 91, 94, 96 and 105 were obtained at steps15, 16, 17, 18, 20 and 21 similarly as EC-87 (Supplementary Table S7).

smFRET experiments and data analysis

0.5 μM Cy3Cy5-riboG-apt, Cy3Cy5-riboG-term or Cy3Cy5-full-length riboG were hybridized with 0.75 μM biotinylated 13 nt-DNA by incubating at 90 °C for 5 min and then cooled to room temperature in the T50 buffer (10 mM Tris-HCl, 50 mM NaCl, pH 8.0). The sequence of the biotinylated DNA is listed in Supplementary Table S1. The hybridized Cy3Cy5-labeled RNA was then diluted to 10~100 pM for the subsequent smFRET measurements. Polymer-coated quartz slides were immersed at the 0.1 mg/μL biotin-PEG and 0.3 mg/μL m-PEG for 2 h (Roy et al., 2008), then coated with 0.2 mg/mL streptavidin for 5 min. 10~100 pM Cy3Cy5-labeled RNA or ECs in the

buffer (10 mM Tris-HCl, 50 mM NaCl, 0~100 mM guanidine, 0~100 mM Mg^{2+}) was injected and then rinsed 3 times to remove the free RNA or ECs. 3 mM Trolox (MCE, USA), 5 mM 3,4-protocatechuic acid (PCA, Shanghai Aladdin Bio-Chem Technology Co., China) and 5 nM protocatechuate dioxygenase (PCD) was added to reduce the photobleaching (Aitken et al., 2008). smFRET experiments were performed by using an objective-type total internal reflection fluorescence (TRIF) microscopy and an inverted microscope (Eclipse Ti, Nikon, Japan) at 20 °C, with FRET marker dyes Cy3 (donor) and Cy5 (acceptor) was excited by 532 nm and 640 nm laser, respectively. Open-sourced software iSMS (Preus et al., 2015) was used to process the single-molecule videos to extract the time-dependent signals. Time resolution of 100 ms was used for each single-molecule video collection excepted noted. Single-molecule trajectories were identified by Deep FRET (Thomsen et al., 2020). The FRET efficiency, E_{FRET} was calculated using the equation:

$$E_{FRET} = I_A/(I_A+I_D).$$

Where I_A and I_D are acceptor and donor fluorescence intensity, respectively. We used empirical Bayesian method of the hidden Markov modelling (HMM) package vbFRET to estimate the FRET states and the time points of transitions (Bronson et al., 2009). The transition density plots (TDP) were plotted by Python module matplotlib, and the lifetimes were plotted in histogram and fitted with a simple exponential decay function by Origin 8.5 to obtain the rate constants. The relative free energy, $\Delta\Delta G$ was measured using the equation $\Delta\Delta G_{ab} = -RT \ln(P_b/P_a)$, where R, T, P_a and P_b are the gas constant, absolute temperature, population of the observed state b and population of the control state a, respectively (Manz et al., 2017).

In vitro transcription termination assay

The single-round transcription termination assay was carried out by PLOR (Chien et al., 2023). The detailed procedure and reagents are listed in Supplementary Tables S8–16. 0~10 mM guanidine and 2~6 mM Mg^{2+} were added at step 8 in Supplementary Tables S8 to measure the effect of guanidine on transcription read-through of the guanidine-IV riboswitch. The products collected at the last step were loaded to 12% denaturing PAGE to compare the transcription read-through efficiencies at different conditions.

Acknowledgements

The work was supported by the National Key Research and Development Program of China [grant no. 2021YFA0910300] and National Natural Science Foundation of China [grant no. 32071300 and 31872628].

Author Contributions

L.G. and Y.L. designed experiments; L.G. collected and analyzed the FRET data; L.G. and D.C. collected *in vitro* data; L.G. and Y.L. drafted the manuscript and all authors contributed to the revision.

Competing Interests

The authors declare no competing interests.

References

1. Aitken C. E., Marshall R. A., Puglisi J. D (2008) **An oxygen scavenging system for improvement of dye stability in single-molecule fluorescence experiments** *Biophys J* **94**:1826–1835 https://doi.org/10.1529/biophysj.107.117689

2. Battaglia R. A., Ke A (2018) **Guanidine-sensing riboswitches: How do they work and what do they regulate?** *Wiley Interdiscip Rev RNA* **9** https://doi.org/10.1002/wrna.1482

3. Binas O., Schamber T., Schwalbe H (2020) **The conformational landscape of transcription intermediates involved in the regulation of the ZMP-sensing riboswitch from Thermosinus carboxydivorans** *Nucleic Acids Res* **48**:6970–6979 https://doi.org/10.1093/nar/gkaa427

4. Breaker R. R (2022) **The Biochemical Landscape of Riboswitch Ligands** *Biochemistry* **61**:137–149 https://doi.org/10.1021/acs.biochem.1c00765

5. Bronson J. E., Fei J., Hofman J. M., Gonzalez R. L., Wiggins C. H (2009) **Learning Rates and States from Biophysical Time Series: A Bayesian Approach to Model Selection and Single-Molecule FRET Data** *Biophysical Journal* **97**:3196–3205 https://doi.org/10.1016/j.bpj.2009.09.031

6. Chien P.-Y., Gao L., Liu Y (2023) **Quantitative Analysis of Transcription Termination via Position-Selective Labeling of RNA (PLOR) Method** *International Journal of Molecular Sciences* **24** https://doi.org/10.3390/ijms24054934

7. Durniak K. J., Bailey S., Steitz T. A (2008) **The structure of a transcribing T7 RNA polymerase in transition from initiation to elongation** *Science* **322**:553–557 https://doi.org/10.1126/science.1163433

8. Frieda K. L., Block S. M (2012) **Direct Observation of Cotranscriptional Folding in an Adenine Riboswitch** *Science* **338**:397–400 https://doi.org/10.1126/science.1225722

9. Garst A. D., Edwards A. L., Batey R. T (2011) **Riboswitches: structures and mechanisms** *Cold Spring Harb Perspect Biol* **3** https://doi.org/10.1101/cshperspect.a003533

10. Helmling C., Wacker A., Wolfinger M. T., Hofacker I. L., Hengesbach M., Furtig B., Schwalbe H (2017) **NMR Structural Profiling of Transcriptional Intermediates Reveals Riboswitch Regulation by Metastable RNA Conformations** *J Am Chem Soc* **139**:2647–2656 https://doi.org/10.1021/jacs.6b10429

11. Hua B., Jones C. P., Mitra J., Murray P. J., Rosenthal R., Ferre-D'Amare A. R., Ha T (2020) **Real-time monitoring of single ZTP riboswitches reveals a complex and kinetically controlled decision landscape** *Nature Communications* **11** https://doi.org/10.1038/s41467-020-18283-1

12. Hua B., Panja S., Wang Y., Woodson S. A., Ha T (2018) **Mimicking Co-Transcriptional RNA Folding Using a Superhelicase** *J Am Chem Soc* **140**:10067–10070 https://doi.org/10.1021/jacs.8b03784

13. Huang J., Sousa R (2000) **T7 RNA polymerase elongation complex structure and movement** *Journal of Molecular Biology* **303**:347–358 https://doi.org/10.1006/jmbi.2000.4150

14. Huang L., Wang J., Lilley D. M. J (2017) **The Structure of the Guanidine-II Riboswitch** *Cell Chem Biol* **24**:695–702 https://doi.org/10.1016/j.chembiol.2017.05.014

15. Huang L., Wang J., Wilson T. J., Lilley D. M. J (2017) **Structure of the Guanidine III Riboswitch** *Cell Chemical Biology* **24**:1407–1415 https://doi.org/10.1016/j.chembiol.2017.08.021

16. Jones C. P., Ferre-D'Amare A. R (2017) **Long-Range Interactions in Riboswitch Control of Gene Expression** *Annu Rev Biophys* **46**:455–481 https://doi.org/10.1146/annurev-biophys-070816-034042

17. Kavita K., Breaker R. R (2023) **Discovering riboswitches: the past and the future** *Trends Biochem Sci* **48**:119–141 https://doi.org/10.1016/j.tibs.2022.08.009

18. Kermani A. A., Macdonald C. B., Gundepudi R., Stockbridge R. B (2018) **Guanidinium export is the primal function of SMR family transporters** *Proc Natl Acad Sci U S A* **115**:3060–3065 https://doi.org/10.1073/pnas.1719187115

19. Landgraf T., Volklein A. E., Furtig B., Schwalbe H (2022) **The cotranscriptional folding landscape for two cyclic di-nucleotide-sensing riboswitches with highly homologous aptamer domains acting either as ON- or OFF-switches** *Nucleic Acids Res* **50**:6639–6655 https://doi.org/10.1093/nar/gkac514

20. Lenkeit F., Eckert I., Hartig J. S., Weinberg Z (2020) **Discovery and characterization of a fourth class of guanidine riboswitches** *Nucleic Acids Res* **48**:12889–12899 https://doi.org/10.1093/nar/gkaa1102

21. Liu Y., Holmstrom E., Yu P., Tan K., Zuo X., Nesbitt D. J., Sousa R., Stagno J. R., Wang Y. X (2018) **Incorporation of isotopic, fluorescent, and heavy-atom-modified nucleotides into RNAs by position-selective labeling of RNA** *Nat Protoc* **13**:987–1005 https://doi.org/10.1038/nprot.2018.002

22. Liu Y. *et al.* (2015) **Synthesis and applications of RNAs with position-selective labelling and mosaic composition** *Nature* **522**:368–372 https://doi.org/10.1038/nature14352

23. Lou Y., Woodson S. A (2024) **Co-transcriptional folding of the glmS ribozyme enables a rapid response to metabolite** *Nucleic Acids Research* **52**:872–884 https://doi.org/10.1093/nar/gkad1120

24. Lubkowska L., Maharjan A. S., Komissarova N (2011) **RNA Folding in Transcription Elongation Complex** *Journal of Biological Chemistry* **286**:31576–31585 https://doi.org/10.1074/jbc.M111.249359

25. Mandal M., Breaker R. R (2004) **Gene regulation by riboswitches** *Nat Rev Mol Cell Biol* **5**:451–463 https://doi.org/10.1038/nrm1403

26. Manz C., Kobitski A. Y., Samanta A., Keller B. G., Jaschke A., Nienhaus G. U (2017) **Single-molecule FRET reveals the energy landscape of the full-length SAM-I riboswitch** *Nat Chem Biol* **13**:1172–1178 https://doi.org/10.1038/nchembio.2476

27. McCown P. J., Corbino K. A., Stav S., Sherlock M. E., Breaker R. R (2017) **Riboswitch diversity and distribution** *Rna* **23**:995–1011 https://doi.org/10.1261/rna.061234.117

28. Nelson J. W., Atilho R. M., Sherlock M. E., Stockbridge R. B., Breaker R. R (2017) **Metabolism of Free Guanidine in Bacteria Is Regulated by a Widespread Riboswitch Class** *Mol Cell* **65**:220–230 https://doi.org/10.1016/j.molcel.2016.11.019

29. Preus S., Noer S. L., Hildebrandt L. L., Gudnason D., Birkedal V (2015) **iSMS: single-molecule FRET microscopy software** *Nat Methods* **12**:593–594 https://doi.org/10.1038/nmeth.3435

30. Reiss C. W., Strobel S. A (2017) **Structural basis for ligand binding to the guanidine-II riboswitch** *Rna* **23**:1338–1343 https://doi.org/10.1261/rna.061804.117

31. Roy R., Hohng S., Ha T (2008) **A practical guide to single-molecule FRET** *Nat Methods* **5**:507–516 https://doi.org/10.1038/nmeth.1208

32. Salvail H., Balaji A., Yu D., Roth A., Breaker R. R (2020) **Biochemical Validation of a Fourth Guanidine Riboswitch Class in Bacteria** *Biochemistry* **59**:4654–4662 https://doi.org/10.1021/acs.biochem.0c00793

33. Serganov A., Nudler E (2013) **A decade of riboswitches** *Cell* **152**:17–24 https://doi.org/10.1016/j.cell.2012.12.024

34. Sherlock M. E., Breaker R. R (2020) **Former orphan riboswitches reveal unexplored areas of bacterial metabolism, signaling, and gene control processes** *Rna* **26**:675–693 https://doi.org/10.1261/rna.074997.120

35. Sherwood A. V., Henkin T. M (2016) **Riboswitch-Mediated Gene Regulation: Novel RNA Architectures Dictate Gene Expression Responses** *Annu Rev Microbiol* **70**:361–374 https://doi.org/10.1146/annurev-micro-091014-104306

36. Strobel E. J., Cheng L., Berman K. E., Carlson P. D., Lucks J. B (2019) **A ligand-gated strand displacement mechanism for ZTP riboswitch transcription control** *Nat Chem Biol* **15**:1067–1076 https://doi.org/10.1038/s41589-019-0382-7

37. Tahirov T. H., Temiakov D., Anikin M., Patlan V., McAllister W. T., Vassylyev D. G., Yokoyama S (2002) **Structure of a T7 RNA polymerase elongation complex at 2.9 A resolution** *Nature* **420**:43–50 https://doi.org/10.1038/nature01129

38. Thomsen J., Sletfjerding M. B., Jensen S. B., Stella S., Paul B., Malle M. G., Montoya G., Petersen T. C., Hatzakis N. S (2020) **DeepFRET, a software for rapid and automated single-molecule FRET data classification using deep learning** *eLife* **9** https://doi.org/10.7554/eLife.60404

39. Uhm H., Kang W., Ha K. S., Kang C., Hohng S (2018) **Single-molecule FRET studies on the cotranscriptional folding of a thiamine pyrophosphate riboswitch** *Proc Natl Acad Sci U S A* **115**:331–336 https://doi.org/10.1073/pnas.1712983115

40. Wang S., Chen D., Gao L., Liu Y (2022) **Short Oligonucleotides Facilitate Co-transcriptional Labeling of RNA at Specific Positions** *Journal of the American Chemical Society* **144**:5494–5502 https://doi.org/10.1021/jacs.2c00020

41. Wickiser J. K., Winkler W. C., Breaker R. R., Crothers D. M (2005) **The speed of RNA transcription and metabolite binding kinetics operate an FMN riboswitch** *Mol Cell* **18**:49–60 https://doi.org/10.1016/j.molcel.2005.02.032

42. Widom J. R., Nedialkov Y. A., Rai V., Hayes R. L., Brooks C. L, Artsimovitch I., Walter N. G. (2018) **Ligand Modulates Cross-Coupling between Riboswitch Folding and Transcriptional Pausing** *Mol Cell* **72**:541–552 https://doi.org/10.1016/j.molcel.2018.08.046

43. Winkler W. C., Breaker R. R (2003) **Genetic control by metabolite-binding riboswitches** *Chembiochem* **4**:1024–1032 https://doi.org/10.1002/cbic.200300685

44. Xue Y., Li J., Chen D., Zhao X., Hong L., Liu Y (2023) **Observation of structural switch in nascent SAM-VI riboswitch during transcription at single-nucleotide and single-molecule resolution** *Nature Communications* **14** https://doi.org/10.1038/s41467-023-38042-2

45. Yadav R., Widom J. R., Chauvier A., Walter N. G (2022) **An anionic ligand snap-locks a long-range interaction in a magnesium-folded riboswitch** *Nature Communications* **13** https://doi.org/10.1038/s41467-021-27827-y

46. Yin Y. W., Steitz T. A (2002) **Structural basis for the transition from initiation to elongation transcription in T7 RNA polymerase** *Science* **298**:1387–1395 https://doi.org/10.1126/science.1077464

47. Zhao B., Guffy S. L., Williams B., Zhang Q (2017) **An excited state underlies gene regulation of a transcriptional riboswitch** *Nat Chem Biol* **13**:968–974 https://doi.org/10.1038/nchembio.2427

48. Zuker M (2003) **Mfold web server for nucleic acid folding and hybridization prediction** *Nucleic Acids Research* **31**:3406–3415 https://doi.org/10.1093/nar/gkg595

Editors

Reviewer #1 (Public Review):

Summary:

This work presents an in-depth characterization of the factors that influence the structural dynamics of the Clostridium botulinum guanidine-IV riboswitch (riboG). Using a single-molecule FRET, the authors demonstrate that riboG undergoes ligand and Mg2+ dependent conformational changes consistent with dynamic formation of a kissing loop (KL) in the aptamer domain. Formation of the KL is attenuated by Mg2+ and Gua+ ligand at physiological concentrations as well as the length of the RNA. Interestingly, the KL is most stable in the context of just the aptamer domain compared to longer RNAs capable of forming the terminator stem. To attenuate transcription, binding of Gua+ and formation of the KL must occur rapidly after transcription of the aptamer domain but before transcription of the rest of the terminator stem.

Strengths:

(1) Single molecule FRET microscopy is well suited to unveil the conformational dynamics of KL formation and the authors provide a wealth of data to examine the effect of the ligand and

ions on riboswitch dynamics. The addition of complementary transcriptional readthrough assays provides further support the author's proposed model of how the riboswitch dynamics contribute to function.
(2) The single-molecule data strongly support that the effect of Gua+ ligand and Mg2+ influence the RNA structure differently for varying lengths of the RNA. The authors also demonstrate that this is specific for Mg2+ as Na+ and K+ ions have little effect.
(3) The PLOR method utilized is clever and well adapted for both dual labeling of RNAs and examining RNA at various lengths to mimic co-transcriptional folding. Using PLOR, they demonstrate that a change in the structural dynamics and ligand binding can occur after extension of the RNA transcript by a single nucleotide. Such a tight window of regulation has intriguing implications for kinetically controlled riboswitches.
(4) In the revised version, the authors utilized multiple destabilizing and compensatory mutations to strengthen their structural interpretation of the KL structure and dynamics and cementing their conclusions.

https://doi.org/10.7554/eLife.94706.2.sa2

Reviewer #2 (Public Review):

Summary:

Gao et al., used single-molecule FRET and step-wise transcription methods to study the conformations of the recently reported guanidine-IV class of bacterial riboswitches that upregulate transcription in the presence of elevated guanidine. Using three riboswitch lengths, the authors analyzed the distributions and transitions between different conformers in response to different Mg2+ and guanidine concentrations. These data led to a three-state kinetic model for the structural switching of this novel class of riboswitches whose structures remain unavailable. Using the PLOR method that the authors previously invented, they further examined the conformations, ligand responses, and gene-regulatory outcomes at discrete transcript lengths along the path of vectorial transcription. These analyses uncover that the riboswitch exhibits differential sensitivity to ligand-induced conformational switching at different steps of transcription, and identify a short window where the regulatory outcome is most sensitive to ligand binding.

Strengths:

Dual internal labeling of long RNA transcripts remains technically very challenging, but essential for smFRET analyses of RNA conformations. The authors should be commended for achieving very highly quality and purity in their labelled RNA samples. The data are extensive, robust, thorough, and meticulously controlled. The interpretations are logical and conservative. The writing is reasonably clear and illustrations are of high quality. The findings are significant because the paradigm uncovered here for this relatively simple riboswitch class is likely also employed in numerous other kinetically regulated riboswitches. The ability to quantitatively assess RNA conformations and ligand responses at multiple discrete points along the path towards the full transcript provides a rare and powerful glimpse into co-transcriptional RNA folding, ligand-binding, and conformational switching.

Weaknesses:

The use of T7 RNA polymerase instead of a near cognate bacterial RNA polymerase in the termination/antitermination assays is a significant caveat. It is understandable as T7 RNA polymerase is much more robust than its bacterial counterparts, which probably will not survive the extensive washes required by the PLOR method. The major conclusions should still hold, as the RNA conformations are probed by smFRET at static, halted complexes instead of on the fly. However, potential effects of the cognate RNA polymerase cannot be discerned

here, including transcriptional rates, pausing, and interactions between the nascent transcript and the RNA exit channel, if any. The authors should refrain from discussing potential effects from the DNA template or the T7 RNA polymerase, as these elements are not cognate with the riboswitch under study.

https://doi.org/10.7554/eLife.94706.2.sa1

Reviewer #3 (Public Review):

Summary:

In this article, Gao et. al. uses single-molecule FRET (smFRET) and position-specific labelling of RNA (PLOR) to dissect the folding and behavioral ligand sensing of the Guanidine-IV riboswitch in the presence and absence of the ligand guanidine and the cation Mg2+. Results provided valuable information on the mechanistic aspects of the riboswitch, including the confirmation on the kissing loop present in the structure as essential for folding and riboswitch activity. Co-transcriptional investigations of the system provided key information on the ligand-sensing behavior and ligand-binding window of the riboswitch. A plausible folding model of the Guanidine-IV riboswitch was proposed as a final result. The evidence presented here sheds additional light into the mode of action of transcriptional riboswitches.

Strengths:

The investigations were very thorough, providing data that supports the conclusions. The use of smFRET and PLOR to investigate RNA folding has been shown to be a valuable tool to the understand of folding and behavior properties of these structured RNA molecules. The co-transcriptional analysis brought important information on how the riboswitch works, including the ligand-sensing and the binding window that promotes the structural switch. The fact that investigations were done with the aptamer domain, aptamer domain + terminator/anti-terminator region, and the full length riboswitch were essential to inform how each domain contributes to the final structural state if in the presence of the ligand and Mg2+.

Weaknesses:

The system has its own flaws when comparing to physiological conditions. The RNA polymerase used (the study uses T7 RNA polymerase) is different from the bacterial RNA polymerase, not only on complexity, but also in transcriptional speed, that can direct interfere with folding and ligand-sensing. Additionally, rNTPs concentrations were much lower than physiological concentrations during transcription, likely causing a change in the polymerase transcriptional speed. These important aspects and how they could interfere with results are important to be addressed to the broad audience. Another point of consideration to be aware is that the bulky fluorophores attached to the nucleotides can interfere with folding to some extent.

https://doi.org/10.7554/eLife.94706.2.sa0

Author response:

The following is the authors' response to the original reviews.

Public Reviews:

Reviewer #1 (Public Review):

Summary:

This work presents an in-depth characterization of the factors that influence the structural dynamics of the Clostridium botulinum guanidine-IV riboswitch (riboG). Using a single-molecule FRET, the authors demonstrate that riboG undergoes ligand and Mg2+ dependent conformational changes consistent with the dynamic formation of a kissing loop (KL) in the aptamer domain. Formation of the KL is attenuated by Mg2+ and Gua+ ligand at physiological concentrations as well as the length of the RNA. Interestingly, the KL is most stable in the context of just the aptamer domain compared to longer RNAs capable of forming the terminator stem. To attenuate transcription, binding of Gua+ and formation of the KL must occur rapidly after transcription of the aptamer domain but before transcription of the rest of the terminator stem.

Strengths:

(1) Single-molecule FRET microscopy is well suited to unveil the conformational dynamics of KL formation and the authors provide a wealth of data to examine the effect of the ligand and ions on riboswitch dynamics. The addition of complementary transcriptional readthrough assays provides further support for the author's proposed model of how the riboswitch dynamics contribute to function.

(2) The single-molecule data strongly support that the effect of Gua+ ligand and Mg2+ influence the RNA structure differently for varying lengths of the RNA. The authors also demonstrate that this is specific for Mg2+ as Na+ and K+ ions have little effect.

(3) The PLOR method utilized is clever and well adapted for both dual labeling of RNAs and examining RNA at various lengths to mimic co-transcriptional folding. Using PLOR, they demonstrate that a change in the structural dynamics and ligand binding can occur after the extension of the RNA transcript by a single nucleotide. Such a tight window of regulation has intriguing implications for kinetically controlled riboswitches.

Weaknesses:

(1) The authors use only one mutant to confirm that their FRET signal indicates the formation of the KL. Importantly, this mutation does not involve the nucleotides that are part of the KL interaction. It would be more convincing if the authors used mutations in both strands of the KL and performed compensatory mutations that restore base pairing. Experiments like this would solidify the structural interpretation of the work, particularly in the context of the full-length riboG RNA or in the cotranscriptional mimic experiments, which appear to have more conformational heterogeneity.

We thank the reviewer for describing our work “in-depth characterization” of riboG. We agree with the reviewer and we have added two more mutants, G71C and U72C with the mutations located at the KL (Figure 2– figure supplement 8A, 8B, 9A, 9B, Figure 3– figure supplement 6A, 6B, 7A, 7B, and Figure 4– figure supplement 6A, 6B, 7A, 7B). Furthermore, we have performed compensatory mutations, C30G-G71C and A29G-U72C that restore base pairing in the KL (Figure 2– figure supplement 8C, 8D, 9C, 9D, Figure 3– figure supplement 6C, 6D, 7C, 7D, and Figure 4– figure supplement 6C, 6D, 7C, 7D). We added the experimental results in the revised manuscript accordingly as “The highly conserved nucleotides surrounding the KL are crucial for its formation (Lenkeit et al., 2020). To test our hypothesis that the state with EFRET ~ 0.8 corresponds to the conformation with the KL, we preformed smFRET analysis on several mutations at these crucial nucleotides (Figure 2– figure

supplement 8–10). Consistent with our expectations, the peaks with EFRET ~ 0.8 was significantly diminished in the riboG-G71C mutant, which features a single nucleotide mutation at site 71 (with 97% nucleotide conservation) in the KL (Figure 2– figure supplement 8A and 8B). It is worth noting that the C30G and G71C mutant, which were initially expected to restore a base pair in the KL, did not successfully bring about the anticipated peak of EFRET ~ 0.8 (Figure 2– figure supplement 8C and 8D). On the other hand, the riboG-U72C mutant exhibited a lower proportion at the state with EFRET ~ 0.8 than riboG-apt. However, the A29G and U72C mutations restored a base pair in the KL, as well as the formation of the KL (Figure 2– figure supplement 9). Furthermore, our investigation revealed that the G77C mutant, involving a single nucleotide mutation at a highly conversed site, 77 (with 97% nucleotide conservation), also hindered the formation of the KL (Figure 2– figure supplement 10). This finding aligns with previous research (Lenkeit et al., 2020) and the predicted second structure of G77C mutation by Mfold (Zuker, 2003)" (page 7), "In contrast to riboG-term, both its G71C and C30G-G71C mutants displayed a reduced proportion of the state with EFRET ~ 0.8. Remarkably, the fractions of EFRET ~ 0.8 remained unaffected by the addition of 1.0 mM Gua+ in these mutants. Distinct from riboG-term, no structural transitions between states were observed in the two mutants (Figure 3– figure supplement 6). Regarding the U72C mutant of riboG-term, the mutation at the site 72 had a reduced impact on the KL conformation in the presence of 1.0 mM Gua+ and 2.0 mM Mg2+. However, the increased proportion of EFRET ~ 0.8 in the A29G-U72C mutant of riboG-term suggests that these mutations can restore the base-pairing between sites 29 and 72, as well as facilitate the formation of the KL (Figure 3– figure supplement 7)" (page 8), and "Upon comparing the G71C and C30G-G71C mutants of the full-length riboG with their wild-type counterpart, it was observed that the wild-type adopted higher proportions of the state with EFRET ~ 0.8 (Figure 4– figure supplement 6). Regarding the U72C and A29G-U72C mutants of the full-length riboG, their behaviors with regards to the peak with EFRET ~ 0.8 were similar to that of their counterparts in riboG-term (Figure 4– figure supplement 7)" (page 9).

> *(2) The existence of the pre-folded state (intermediate FRET ~0.5) is not well supported in their data and could be explained by an acquisition artifact. The dwell times are very short often only a single frame indicating that there could be a very fast transition (< 0.1s) from low to high FRET that averages to a FRET efficiency of 0.5. To firmly demonstrate that this intermediate FRET state is metastable and not an artifact, the authors need to perform measurements with a faster frame rate and demonstrate that the state is still present.*

We thank the reviewer for the great comment. We added smFRET experiments at higher time resolution, 20 ms, as well as lower time resolution (Figure 2– figure supplement 3). Based on our experimental results, the intermediate state (EFRET ~0.5) exists at the smFRET collected at 20 ms, 100 ms and 200 ms.

> *(3) The PLOR method employs a non-biologically relevant polymerase (T7 RNAP) to mimic transcription elongation and folding near the elongation complex. T7 RNAP has a shorter exit channel than bacterial RNAPs and therefore, folding in the exit channel may be different between different RNAPs. Additionally, the nascent RNA may interact with bacterial RNAP differently. For these reasons, it is not clear how well the dynamics observed in the T7 ECs recapitulate riboswitch folding dynamics in bacterial ECs where they would occur in nature.*

We thank the reviewer for the comment. We agree with the reviewer that the bacterial and T7 RNAPs may behave differently due to their differences in transcriptional speed, dynamics, interactions, and so on. And we added a statement in the Discussion as "It is worth noting that the RNAP utilized in our study is T7 RNAP, which exhibits distinct characteristics compared to bacterial RNAP in terms of transcriptional speed, dynamics, and interactions.

However, Xue et al. have reported similarities between T7 and E. coli RNAP in the folding of nascent RNA. Additionally, Lou and Woodson have provided valuable insights into the co-transcriptional folding of the glmS ribozyme using T7 RNAP (Xue et al., 2023; Lou & Woodson, 2024)" (page 13–14).

> ***Reviewer #2 (Public Review):***
>
> *Summary:*
>
> *Gao et al. used single-molecule FRET and step-wise transcription methods to study the conformations of the recently reported guanidine-IV class of bacterial riboswitches that upregulate transcription in the presence of elevated guanidine. Using three riboswitch lengths, the authors analyzed the distributions and transitions between different conformers in response to different Mg2+ and guanidine concentrations. These data led to a three-state kinetic model for the structural switching of this novel class of riboswitches whose structures remain unavailable. Using the PLOR method that the authors previously invented, they further examined the conformations, ligand responses, and gene-regulatory outcomes at discrete transcript lengths along the path of vectorial transcription. These analyses uncover that the riboswitch exhibits differential sensitivity to ligand-induced conformational switching at different steps of transcription, and identify a short window where the regulatory outcome is most sensitive to ligand binding.*
>
> *Strengths:*
>
> *Dual internal labeling of long RNA transcripts remains technically very challenging but essential for smFRET analyses of RNA conformations. The authors should be commended for achieving very high quality and purity in their labelled RNA samples. The data are extensive, robust, thorough, and meticulously controlled. The interpretations are logical and conservative. The writing is reasonably clear and the illustrations are of high quality. The findings are significant because the paradigm uncovered here for this relatively simple riboswitch class is likely also employed in numerous other kinetically regulated riboswitches. The ability to quantitatively assess RNA conformations and ligand responses at multiple discrete points along the path towards the full transcript provides a rare and powerful glimpse into cotranscriptional RNA folding, ligand-binding, and conformational switching.*
>
> *Weaknesses:*
>
> *The use of T7 RNA polymerase instead of a near-cognate bacterial RNA polymerase in the termination/antitermination assays is a significant caveat. It is understandable as T7 RNA polymerase is much more robust than its bacterial counterparts, which probably will not survive the extensive washes required by the PLOR method. The major conclusions should still hold, as the RNA conformations are probed by smFRET at static, halted complexes instead of on the fly. However, potential effects of the cognate RNA polymerase cannot be discerned here, including transcriptional rates, pausing, and interactions between the nascent transcript and the RNA exit channel, if any. The authors should refrain from discussing potential effects from the DNA template or the T7 RNA polymerase, as these elements are not cognate with the riboswitch under study.*

We thank the reviewer for describing our work "The data are extensive, robust, thorough, and meticulously controlled. The interpretations are logical and conservative. The writing is reasonably clear and the illustrations are of high quality". We agree with the reviewer that the bacterial and T7 RNAPs may behave differently due to their differences in transcriptional speed, dynamics, interactions, and so on. And we added a statement in the Discussion as "It is worth noting that the RNAP utilized in our study is T7 RNAP, which exhibits distinct

characteristics compared to bacterial RNAP in terms of transcriptional speed, dynamics, and interactions. However, Xue et al. have reported similarities between T7 and E. coli RNAP in the folding of nascent RNA. Additionally, Lou and Woodson have provided valuable insights into the co-transcriptional folding of the glmS ribozyme using T7 RNAP (Xue et al., 2023; Lou & Woodson, 2024)" (page 14).

> ***Reviewer #3 (Public Review):***
>
> *Summary:*
>
> *In this article, Gao et. al. uses single-molecule FRET (smFRET) and position-specific labelling of RNA (PLOR) to dissect the folding and behavioral ligand sensing of the Guanidine-IV riboswitch in the presence and absence of the ligand guanidine and the cation Mg2+. The results provided valuable information on the mechanistic aspects of the riboswitch, including the confirmation of the kissing loop present in the structure as essential for folding and riboswitch activity. Co-transcriptional investigations of the system provided key information on the ligand-sensing behavior and ligandbinding window of the riboswitch. A plausible folding model of the Guanidine-IV riboswitch was proposed as a final result. The evidence presented here sheds additional light on the mode of action of transcriptional riboswitches.*
>
> *Strengths:*
>
> *The investigations were very thorough, providing data that supports the conclusions. The use of smFRET and PLOR to investigate RNA folding has been shown to be a valuable tool for the understanding of folding and behavior properties of these structured RNA molecules. The co-transcriptional analysis brought important information on how the riboswitch works, including the ligand-sensing and the binding window that promotes the structural switch. The fact that investigations were done with the aptamer domain, aptamer domain + terminator/anti-terminator region, and the full-length riboswitch were essential to inform how each domain contributes to the final structural state if in the presence of the ligand and Mg2+.*
>
> *Weaknesses:*
>
> *The system has its own flaws when compared to physiological conditions. The RNA polymerase used (the study uses T7 RNA polymerase) is different from the bacterial RNA polymerase, not only in complexity, but also in transcriptional speed, which can directly interfere with folding and ligand-sensing. Additionally, rNTPs concentrations were much lower than physiological concentrations during transcription, likely causing a change in the polymerase transcriptional speed. These important aspects and how they could interfere with results are important to be addressed to the broad audience. Another point of consideration to be aware of is that the bulky fluorophores attached to the nucleotides can interfere with folding to some extent.*

We thank the reviewer for describing our work as "The investigations were very thorough, providing data that supports the conclusions". We agree with the reviewer that the bacterial and T7 RNAPs may behave differently due to their differences in transcriptional speed, dynamics, interactions, and so on. And we added a statement in the Discussion as "It is worth noting that the RNAP utilized in our study is T7 RNAP, which exhibits distinct characteristics compared to bacterial RNAP in terms of transcriptional speed, dynamics, and interactions. However, Xue et al. have reported similarities between T7 and E. coli RNAP in the folding of nascent RNA. Additionally, Lou and Woodson have provided valuable insights into the cotranscriptional folding of the glmS ribozyme using T7 RNAP (Xue et al., 2023; Lou & Woodson, 2024)" (page 14). And we also agree with the reviewer that the lower NTP may

affect the transcriptional speed. Regarding the fluorophores, we purposely placed them away from the KL to avoid their influence on the formation of the KL.

> ***Reviewer #1 (Recommendations For The Authors):***
>
> *Related to weakness 1*
>
> *- The authors cite a paper that investigated mutations in the KL duplex but do not include these mutations in their analysis. It is unclear why the authors chose the G77C mutation and not the other mutants previously tested. Can the authors explain their choice of mutation in detail in the text? I also did not see the proposed secondary structure for the G77C mutant shown in Figure 2 -supp 3A in the cited paper, is this a predicted structure? Please explain how this structure was determined.*

We thank the reviewer for the comment. The reason we chosen the G77C mutation is based on previous report that G77C can disturb the formation of the KL, as we stated in the manuscript as “Furthermore, our investigation revealed that the G77C mutant, involving a single nucleotide mutation at a highly conversed site, 77 (with 97% nucleotide conservation), also hindered the formation of the KL (Figure 2– figure supplement 10). This finding aligns with previous research (Lenkeit et al., 2020) and the predicted second structure of G77C mutation by Mfold (Zuker, 2003)” (page 7). And the secondary structure for the G77C mutant was predicted by Mfold, which as cited in the manuscript and added in the reference list as “Zuker, M. (2003). Mfold web server for nucleic acid folding and hybridization prediction. Nucleic Acids Research, 31(13), 3406-3415”.

> *- It is not clear to me that the structural interpretation of their FRET states is correct and that the FRET signal reports on the base pairing of the KL in only the high FRET state. The authors should perform experiments with additional mutations in the KL duplex to confirm that their construct reports on KL duplex formation alone and not other structural dynamics.*

We thank the reviewer for the comment. We have included additional mutations to establish a connection between the high-FRET state to the formation of the KL. The results have been added to the manuscript as “The highly conserved nucleotides surrounding the KL are crucial for its formation (Lenkeit et al., 2020). To test our hypothesis that the state with EFRET ~ 0.8 corresponds to the conformation with the KL, we preformed smFRET analysis on several mutations at these crucial nucleotides (Figure 2– figure supplement 8–10). Consistent with our expectations, the peaks with EFRET ~ 0.8 was significantly diminished in the riboG-G71C mutant, which features a single nucleotide mutation at site 71 (with 97% nucleotide conservation) in the KL (Figure 2– figure supplement 8A and 8B). It is worth noting that the C30G and G71C mutant, which were initially expected to restore a base pair in the KL, did not successfully bring about the anticipated peak of EFRET ~ 0.8 (Figure 2– figure supplement 8C and 8D). On the other hand, the riboG-U72C mutant exhibited a lower proportion at the state with EFRET ~ 0.8 than riboG-apt. However, the A29G and U72C mutations restored a base pair in the KL, as well as the formation of the KL (Figure 2– figure supplement 9). Furthermore, our investigation revealed that the G77C mutant, involving a single nucleotide mutation at a highly conversed site, 77 (with 97% nucleotide conservation), also hindered the formation of the KL (Figure 2– figure supplement 10). This finding aligns with previous research (Lenkeit et al., 2020) and the predicted second structure of G77C mutation by Mfold (Zuker, 2003)” (page 7), “In contrast to riboG-term, both its G71C and C30G-G71C mutants displayed a reduced proportion of the state with EFRET ~ 0.8. Remarkably, the fractions of EFRET ~ 0.8 remained unaffected by the addition of 1.0 mM Gua+ in these mutants. Distinct from riboG-term, no structural transitions between states were observed in the two mutants (Figure 3– figure supplement 6). Regarding the U72C mutant of riboG-term, the mutation at the site 72 had a reduced impact on the KL conformation in the presence of 1.0 mM Gua+ and 2.0 mM Mg2+.

However, the increased proportion of EFRET ~ 0.8 in the A29G-U72C mutant of riboG-term suggests that these mutations can restore the base-pairing between sites 29 and 72, as well as facilitate the formation of the KL (Figure 3– figure supplement 7)" (page 8), and "Upon comparing the G71C and C30G-G71C mutants of the full-length riboG with their wild-type counterpart, it was observed that the wild-type adopted higher proportions of the state with EFRET ~ 0.8 (Figure 4– figure supplement 6). Regarding the U72C and A29G-U72C mutants of the full-length riboG, their behaviors with regards to the peak with EFRET ~ 0.8 were similar to that of their counterparts in riboG-term (Figure 4– figure supplement 7)" (page 9).

> *- For the full-length riboG-136 (Cy3Cy5 riboG in Figure 4), the authors have clearly defined peaks at 0.6 and 0.4. However, the authors do not explain their structural interpretation of these states. Do the authors believe that the KL is forming in these states? It would be helpful to have data on mutations in the KL in the context of the full-length riboG to better understand the structural transitions of these intermediate states.*

Based on our mutation studies, we proposed that the peak with EFRET ~0.8 corresponds to the conformation with the KL, while the states with EFRET ~0.4 and 0.6 are the states without a stable KL.

> *Related to weakness 2:*
>
> *- For the riboG-apt and riboG-term RNAs, the proposed intermediate FRET state (EFRET = 0.5) is poorly fit by a Gaussian and the dwell times in the state are almost entirely single-frame dwells. It is likely that this state is the result of a camera blurring artifact, in which RNAs undergo a FRET transition between two frames giving an apparent FRET efficiency which is between that of the two transitioning states. This artifact arises when the average dwell times of the true states (Elow and Ehigh) are comparable to the frame duration (within a factor of ~5-10; see https://doi.org/10.1021/acs.jpcb.1c01036). To confirm the presence of the intermediate state, the authors should perform at least a few experiments with higher time resolution to support the existence of the 0.5 state with a lifetime of 0.1 s. Alternatively, the data should be refit to a two-state HMM and the authors could explain in the text that the density in the FRET histogram between the two states is likely due to transitions that are faster than the time resolution of the experiment.*

We thank the reviewer for the great comment. Taking the suggestion into consideration, we performed smFRET experiments with a higher time resolution of 20 ms. As a result, we still detected the intermediate state, supporting that it is not an artifact. The new data has been included in the revised manuscript (Figure 2-figure supplement 3).

> *Related to weakness 3:*
>
> *- The authors depict the polymerase footprint differently in some of the figures and it is unclear if this is part of their model. Is the cartoon RNAP supposed to indicate the RNA:DNA hybrid or the footprint of T7 RNAP on the RNA? For example, in Figure 8a there are 8 nts (left) and 9 nts (right) covered by RNAP, and only 6nts in Figure 6 - supp 2A. This is particularly misleading for the EC-87 and EC-88 in Figure 6 - supp 2, where it is likely that this stem is not formed at all and the KL strand is single-stranded. The authors should clarify and at least indicate in the figure legend if the RNAP cartoon is part of the model or only a representation.*

We thank the reviewer for bringing the issues to our attention. Due to space limitations, we chose to represent the polymerase footprint differently in Figure 8. However, we have included the statement "DNA templates from EC-87 to EC-105 are not displayed in the model" in the legend of Figure 8 to avoid the confusion.

Moreover, we have corrected the error of 6 nts Figure 6-supplement figure 2.

> *- With a correct 9 bp RNA:DNA hybrid, the EC-88 construct would not be able to form the top part of the P2 stem and the second half of the KL RNA would be single-stranded. In this case, an interaction between the KL nucleotides would resemble a pseudoknot and not a kissing loop interaction. Can the authors explain if this could explain the heterogeneity they observe in the EC-88 construct compared to the riboGapt RNA?*

Thank the reviewer for the comment. We have added the statement in the revised manuscript as "The T7 RNA polymerase (RNAP) sequestered about 8 nt of the nascent RNA, preventing the EC-88 construct from forming the P2 stem (Durniak et al., 2008; Huang & Sousa, 2000; Lubkowska et al., 2011; Tahirov et al., 2002; Wang et al., 2022; Yin & Steitz, 2002). Consequently, a pseudoknot structure potentially formed instead of the expected KL. This distinction may account for the observed heterogeneity between EC-88 and riboG-apt" (page 11).

> *Other comments:*
>
> *(1) It appears that the FRET histograms in the PLOR experiments (Figure 6 and related figures) only show the fits presumably to highlight the overlays. However, this makes it impossible to determine the goodness of the fit. The authors should instead show the outline of the raw histogram with the fit, or at least show the raw histograms with fits in the supplement.*

We have replaced Figure 6- figure supplements 2-4 to enhance the clarity of the raw and fitted smFRET histograms.

> *(2) The authors should consider including a concluding paragraph to put the results into a larger context. How does the kinetic window compare to other transcriptional riboswitches? Would the authors comment on how the transcription speed compares to the kinetics for the formation of the KL?*

We thank the reviewer for the comment. We have added the comparison of riboG to other transcription riboswitches to the manuscript as "Nevertheless, the ligand-sensitive windows of riboswitches during transcription vary. In a study conducted by Helmling et al. using NMR spectroscopy, they proposed a broad transcriptional window for deoxyguanosine-sensing riboswitches, whereby the ligand binding capability gradually diminishes over several nucleotide lengths (Helmling et al., 2017). However, more recent research by Binas et al. and Landgraf et al. on riboswitches sensing ZMP, c-di-GMP, and c-GAMP revealed a narrow window with a sharp transition in binding capability, even with transcript lengths differing by only one or three nucleotides (Binas et al., 2020; Landgraf et al., 2022). In line with the findings for the c-GAMP-sensing riboswitch, our study on the guanidine-IV riboswitch also demonstrated a sharp transition in binding capability with just a single nucleotide extension" (page 14).

We appreciate the reviewer's comment in comparing the transcription speed to the kinetics of the KL formation. However, we must acknowledge that we have limited kinetic data in this study to confidently make such a comparison.

> *(3) Cy3Cy5 RiboG is a confusing name because it implies that the others are not also Cy3Cy5 labeled. The authors should consider changing the names and being consistent throughout. I suggest full-length riboG or riboG-136.*

We have changed "Cy3Cy5 riboG" to "Cy3Cy5-full-length riboG" (pages 15 and 16).

> *(4) The transcriptional readthrough experiment should be explained when first mentioned in line 109.*

We have added the citation (Chien et al., 2023) of the transcriptional readthrough experiment to the manuscript as “we noted that the transcriptional read-through of the guanidine-IV riboswitch during the single-round PLOR reaction was sensitive to Gua+, exhibiting an apparent EC50 value of 68.7 □ 7.3 μM (Figure 1D) (Chien et al., 2023)” (page 5).

> *(5) Kd values in text should have uncertainties, and the way these uncertainties are obtained should be explained.*

We have added the uncertainties of Kd values in the revised manuscript (page 6) and the legend of Figure 2-supplement 6 as “The percentages of the folded state (EFRET ~ 0.8) of Cy3Cy5-riboG-apt were plotted with the concentrations of Gua+ at 0.5 mM Mg2+, with an apparent Kd of 286.0 □ 18.1 μM in three independent experiments”.

> *(6) The authors mention "strategies" on line 306, but it is unclear what they are referring to. Are the strategies referring to the constructs (EC-87, etc) or Steps 1-8 in the supplemental figure? Please clarify.*

We have clarified the confusion by adding “The detailed procedures of strategies 1-8 were shown in Figure 7–figure supplement 1” to the manuscript (page 12).

> *(7) What are the fraction of dynamic traces versus static traces in the cases for the full-length riboG? This would help depict the structural heterogeneity in the population.*

We have added the fractions of dynamic single-molecule traces of the full-length riboG to Figure 4-supplements 1-5.

> *(8) The labels in Figure 4 (A-E) don't match the caption (A-H).*

We have corrected the error.

> *(9) The coloring of the RNA strands in Figure 4A should be explained in the figure legend. It could be interpreted as multiple strands annealed instead of a continuous strand.*

We have revised the legend of Figure 4A by adding “The full-length riboG contains the aptamer domain (black), terminator (red) and the extended sequence (blue). Cy3 and Cy5 are shown by green and red sparkles, respectively”.

> *(10) Reported quantities and uncertainties should have the same number of decimal places. In many places, the uncertainties likely have too many significant figures, for example, in Figure 5 and related figures.*

We have corrected the significant figures of the uncertainties.

> *(11) In Figure 5, A and B should have the same vertical scale to facilitate comparison.*

We have adjusted Figure 5A to match the vertical scale of Figure 5B in the revised manuscript.

> *(12) In Figure 5C-D, the construct from which those trajectories come should be indicated in the legend.*

We have added the construct to the legend of Figures 5C and D.

> *(13) In Figure 6J, the splines between data points are confusing and can be misleading. They suggest that the data has been fit to a model, but I am not sure if it represents a model. The data points should be colored instead and lines removed.*

We thank the reviewer for the comment. We have changed Figure 6J by coloring the data points and removing the lines to avoid confusion.

> *(14) Line 330 mentions a P2 structure in Figure 8, but there is no such label in Figure. Please clarify.*

We thank the reviewer for the comment and have added P2 to Figure 8.

> ***Reviewer #2 (Recommendations For The Authors):***
>
> *(1) Figure 1B. The authors don't seem to address the role of the blue stem-loop following Stems 1 and 2. Is this element needed at all for gene regulation? Does it impact the conformations or folding of the preceding Stems 1 and 2? It seems feasible to disrupt the stem and see whether there is an impact on riboswitch function.*

We thank the reviewer for the comment. The presence of the sequence which formed blue stem-loop indicates the formation of an anti-terminator conformation in riboG during transcription. Our smFRET data shows that the inclusion of the stem-loop sequence induces additional peaks in the full-length riboG compared to the riboGterm. This indicates that the stem-loop influences the folding of the kissing loop (KL) and potentially also affects the stems 1 and 2.

> *(2) Figure 7 supplement 1, C &D. Maybe I am missing something, but it seems to me in reaction #8 (EC-105, last two lanes), the readthrough percentage is close to 50% based on the gel but plotted in D as 20%. Further, there is a strong effect of guanidine in reaction #8 but that is not reflected in the quantitation in panel D.*

We thank the reviewer for the comment. The observed discrepancy between reaction 8 in (C) and (D) is from the differential handling of the crude product at the last step (step 17) in gel loading for (C), contrasted with the combination of crude products from steps 16 and 17 to calculate the read-through percentage in (D). We have corrected the discrepancy by replacing Figure 7-Supplement figure 1C (now Figure 7C), and revised the legend to include the following clarification: “Taking into consideration that the 17 step-PLOR reaction exhibited a pause within the terminator region, resulting in a significant amount of terminated product at step 16, crude products from steps 16 and 17 were collected for (C) and (D) of the 17 step-PLOR reaction (Lanes 15 and 16 in C)”.

> *(3) Figure 7C is a control that shows the quality of the elongation complexes, which probably should be in the supplement. Instead, in Figure 7 supplement 1, panels C and D are actual experiments and could be moved into the main figure.*

We thank the reviewer for the comment. We made the adjustment.

> *(4) Figure S7D. I would suggest not labelling the RNA polymerase halt/stoppage sites due to NTP deprivation as "pausing sites" because transcriptional pausing has previously been defined as natural sites where the RNA polymerase transiently halts itself, but not due to the lack of the next NTPs. In this case, the elongating complexes were artificially*

> *halted, which is technically not "pausing", as it will not restart/resume on its own without intervention.*

We have changed the “pausing” to “halting”.

> *(5) Figure 7 is titled "In vitro transcriptional performance of riboG." But the data is actually not about the performance of the riboswitch, or how well it functions. I would suggest the authors revise the title. This is mostly about the observed sensitivity window of the riboswitch to ligand-mediated conformational switching.*

We have changed the title of Figure 7 to “Ligand-mediated conformational switching of riboG during transcription”.

> *(6) Figure 7A, the illustration gives the visual impression that there are multiple RNA polymerases on the same DNA template, which is not the case.*

We have revised Figure 7A by adding arrows between RNA polymerases to illustrate the movement of a single RNAP, rather than multiple RNAP on the same template.

> *(7) It could be informative to compare the guanidine-IV riboswitch with the first three classes (I, II, III), to see how their architectures or gene regulatory mechanisms are similar or different.*

We thank the reviewer for the comment. We have added the comparison of the guanidine-IV riboswitch to other three guanidine riboswitches to the manuscript as “The guanidine-IV riboswitch exhibits similarities to the guanidine-I riboswitch in gene regulatory mechanism, functioning as a transcriptional riboswitch. Structurally, it resembles the guanidine-II riboswitch through the formation of loop-loop interactions upon binding to guanidine (Battaglia & Ke, 2018; L. Huang et al., 2017; Lin Huang et al., 2017; Lenkeit et al., 2020; Nelson et al., 2017; Reiss & Strobel, 2017; Salvail et al., 2020)” (page 12).

> ***Reviewer #3 (Recommendations For The Authors):***
>
> *In addition to the public review items, I provide the following recommendations:*
>
> *(1) As a second language speaker, I understand that writing a compelling and concise story may be hard, and we tend to write more than needed or more repetitively. That being said, I do think that the writing could be improved to make it more concise, clear, and avoid repetitions.*

We thank the reviewer for the comment. We re-wrote the abstract and some sentences in the manuscript.

> *(2) In the abstract, instead of saying that "...This lack of understanding has impeded the application of this riboswitch", which makes the statement too strong, perhaps, stating something along the lines of "this understanding would assist the application of this riboswitch", would be a better fit.*

We have re-wrote the abstract, and revised the sentence.

> *(3) Methods should state which RNA polymerase was used. PLOR uses T7 RNA pol, so I assume it was the same.*

We have added the statement “T7 RNAP was utilized in the PLOR and in vitro transcription reactions except noted” in the Methods (page 15).

> *(4) The impact statement says comprehensive structure-function, where perhaps comprehensive folding-function would be more appropriate. We are still missing a lot of structural information about this particular riboswitch.*

We agree with the reviewer, and changed “comprehensive structure-function” to “folding-function” in Impact statement (page 2).

> *(5) Higher Mg2+ concentrations implicated in a lesser extent of the switch of RiboGapt, a sentence talking about it would be useful (how Mg2+ could have promiscuous interaction and interfere with folding).*

We have added the role of higher Mg2+ to the manuscript as “However, at a higher concentration of 50.0 mM Mg2+, the proportion of the pre-folded and unfolded conformations were more prevalent at 50.0 mM Mg2+ than at 20.0 mM Mg2+. This suggests that an excess of Mg2+ may promote the pre-folded and even unfolded conformations” (page 6).

> *(6) In the investigations of RiboG-term and RiboG, seems like that monovalents from the buffer are sufficient to promote secondary structure. A statement commenting on this would benefit the paper and the audience.*

We agree with the reviewer and have accordingly revised the manuscript accordingly by adding “This indicates that monovalent ions in the buffer can facilitate the formation of stable guanidine-IV riboswitch” (page 8).

> *(7) Figure 3. Figure goes to panel E and legend to panel H. G and H colors do not correspond to actual figure colors.*

We made the correction.

> *(8) Figure 4. The same as Figure 3, the panels and figures are divergent.*

We made the correction.

> *(9) During the discussion, stating that the DNA and RNA pol play a role in folding and ligand binding may be excessive. This could be an indirect effect of the transcriptional bubble hindering part of the nascent RNA from folding, which is something intrinsic to any transcription and not specific to this system.*

We agree with the reviewer and deleted the statement about the DNA and RNAP play a role in folding and ligand binding.

> *(10) PLOR is not properly cited. When introduced in the manuscript, please cite the original PLOR paper (Liu et. al. Nature 2015) and additional related papers.*

We cited the original PLOR paper (Liu et al, Nature 2015) and the related papers (Liu et al, Nature Protocols 2018). (pages 4 and 15)

> *(11) The kinetics race of folding and binding could be a little more emphasized in discussion, particularly from the perspective of its physiological importance.*

We agree with the reviewer and deleted the kinetics race of folding and binding from the Discussion part.

https://doi.org/10.7554/eLife.94706.2.sa4